

## REVIEW

[View Article Online](#)  
[View Journal](#) | [View Issue](#)



Cite this: *Ind. Chem. Mater.*, 2024, 2, 514

## Aqueous Zn–CO<sub>2</sub> batteries: a route towards sustainable energy storage

Yanxiu Liu,<sup>a</sup> Junjie Chen,<sup>a</sup> Weichen Li,<sup>b</sup> Yu Zhang,<sup>iD \*a</sup> Xianwei Fu,<sup>b</sup> Erling Li,<sup>b</sup> Shangbin Jin,<sup>iD e</sup> Li-Ming Yang,<sup>f</sup> Zhihong Tian,<sup>\*b</sup> Markus Antonietti<sup>c</sup> and Tianxi Liu<sup>\*d</sup>

In recent years, the concept of rechargeable aqueous Zn–CO<sub>2</sub> batteries has attracted extensive attention owing to their dual functionality of power supply and simultaneous conversion of CO<sub>2</sub> into value-added chemicals or fuels. The state-of-the-art research has been mainly focused on the exploration of working mechanisms and catalytic cathodes but hardly applies an integrative view. Although numerous studies have proven the feasibility of rechargeable aqueous Zn–CO<sub>2</sub> batteries, challenges remain including the low CO<sub>2</sub> conversion efficiency, poor battery capacity, and low energy efficiency. This review systematically summarizes the working principles and devices, and the catalytic cathodes used for Zn–CO<sub>2</sub> batteries. The challenges and prospects in this field are also elaborated, providing insightful guidance for the future development of rechargeable aqueous Zn–CO<sub>2</sub> batteries with high performance.

Received 31st January 2024,  
Accepted 11th April 2024

DOI: 10.1039/d4im00014e

rsc.li/pcm

Keywords: Zn–CO<sub>2</sub> battery; CO<sub>2</sub> reduction reaction; Working mechanism; Electrocatalysts.

<sup>a</sup> School of Mechanical and Power Engineering, East China University of Science and Technology, Shanghai 200237, China. E-mail: [yzhang071@ecust.edu.cn](mailto:yzhang071@ecust.edu.cn)

<sup>b</sup> Engineering Research Center for Nanomaterials, Henan University, Kaifeng 475004, P. R. China. E-mail: [zhihong.tian@henu.edu.cn](mailto:zhihong.tian@henu.edu.cn)

<sup>c</sup> Department of Colloid Chemistry, Max Planck Institute of Colloids and Interfaces, Potsdam 14476, Germany

<sup>d</sup> Key Laboratory of Synthetic and Biological Colloids, Ministry of Education, School of Chemical and Material Engineering, Jiangnan University, Wuxi 214122, P. R. China. E-mail: [txliu@jiangnan.edu.cn](mailto:txliu@jiangnan.edu.cn)

<sup>e</sup> School of Chemical Engineering and Technology, Xi'an Jiaotong University, 28 Xianning Road, Xi'an, Shaanxi, 710049, China

<sup>f</sup> School of Chemistry and Chemical Engineering, Huazhong University of Science and Technology, Wuhan 430074, China



Yanxiu Liu

Yanxiu Liu received her BE degree from Nanjing Tech University in 2020 and ME degree from Yancheng Institute of Technology in 2023. She is currently a PhD candidate under the supervision of Prof. Yu Zhang in the School of Mechanical and Power Engineering at East China University of Science and Technology. Her research mainly focuses on the electrocatalyst synthesis and mechanism studies for metal–CO<sub>2</sub> batteries.



Yu Zhang

Yu Zhang is currently a professor from East China University of Science and Technology (ECUST) in Shanghai, China. She obtained her BS degree from Nanjing University in 2012 and PhD degree from Nanyang Technological University, Singapore in 2017. She then worked as a postdoctoral fellow at the Hong Kong University of Science and Technology and Georgia Institute of Technology. In 2020, she joined the School of Mechanical and Power Engineering in ECUST. Her research expertise lies in the development of electrode materials and devices for rechargeable batteries and electrocatalysis.



photosynthesis) and balancing generation and fixation is an obvious mandate.

This opens the opportunity to tackle those challenges with new global chemical engineering tools or industries. An electrochemical  $\text{CO}_2$  reduction reaction ( $\text{CO}_2\text{RR}$ ) has been recently demonstrated to be an effective strategy to use excess sustainable electricity for upgrading  $\text{CO}_2$  into value-added chemicals (such as  $\text{HCOOH}$  or  $\text{C}_2\text{H}_4$ ).<sup>4–10</sup> Notably, compared with metal-ion or metal-air batteries,<sup>11–16</sup> metal– $\text{CO}_2$  batteries do not only reduce  $\text{CO}_2$  into products of high value but also provide energy during the discharging process, which is regarded as an extra advantage compared to the individual electrochemical  $\text{CO}_2$  conversion.<sup>17,18</sup> Therefore, metal– $\text{CO}_2$  batteries on a larger scale can become a powerful tool for both energy and raw material management.<sup>19,20</sup>

In pioneering work, Takechi *et al.* for the first time reported in 2011 that the capacity of a  $\text{Li}-\text{O}_2$  battery was greatly improved after the introduction of  $\text{CO}_2$  to the gas phase.<sup>21</sup> Subsequently, the batteries using  $\text{CO}_2$  as the working gas received widespread attention.<sup>18,19,22</sup> As for the working mechanism, the Li metal anode gets oxidized and releases electrons to form  $\text{Li}^+$  and  $\text{CO}_2$  gets reduced to  $\text{Li}_2\text{CO}_3$  and C-species during the discharging process;  $\text{Li}_2\text{CO}_3$  and C-species are decomposed or oxidized and release  $\text{CO}_2$  during the charging process.<sup>23,24</sup> However, the practical implementation of  $\text{Li}-\text{CO}_2$  batteries suffers from the complex reaction mechanism, deposition of solid products, and the high cost and safety concerns of organic electrolytes, driving the research community to search for alternative metal– $\text{CO}_2$  batteries.<sup>25,26</sup> Compared with non-aqueous  $\text{Na}/\text{Li}-\text{CO}_2$  batteries,  $\text{Zn}-\text{CO}_2$  batteries possess favorable merits including good safety and low cost due to the use of aqueous electrolytes.<sup>27,28</sup> Besides, the cathodic reaction does not produce solid products during the

discharge process, which is beneficial for improving the cycle life.

Recently, Zn metal has been described as one of the potential candidates for use as the anode in batteries due to its low price, high theoretical capacity ( $825 \text{ mA h g}^{-1}$ ), and the ability to use sustainable aqueous electrolytes.<sup>29,30</sup> The function of aqueous  $\text{Zn}-\text{CO}_2$  batteries involves various simultaneous electrochemical reactions including  $\text{CO}_2\text{RR}$  during the discharging process and oxygen evolution reactions (OER) or the oxidation of liquid products of  $\text{CO}_2\text{RR}$  during the charging process. The advantage of the  $\text{Zn}-\text{CO}_2$  battery is that it could combine  $\text{CO}_2$  reduction and energy storage. However, cathodes are additionally required to inhibit the competitive hydrogen evolution reaction (HER) against the  $\text{CO}_2\text{RR}$  by electrocatalyst design.<sup>31,32</sup> Since Xie *et al.* developed a reversible  $\text{Zn}-\text{CO}_2$  battery using Pd nanosheets as catalysts for the cathode,<sup>33</sup> different types of catalysts have been investigated for rechargeable aqueous  $\text{Zn}-\text{CO}_2$  batteries. For a pre-review, Table 1 summarizes the catalytic cathodes and the performance of recently reported first trials to reach the diverse working units of a  $\text{Zn}-\text{CO}_2$  battery. However, the development of a whole  $\text{Zn}-\text{CO}_2$  battery is still rather the exception, and anodic sides as well as integration into an operative true battery system must be further investigated. Herein, mainly device engineering towards thin-film or flow batteries is discussed, as most work is still done with laboratory-level H-cell set-ups.

This review will cover the reaction mechanisms, battery configurations, and catalytic cathodes of the reported aqueous  $\text{Zn}-\text{CO}_2$  battery, as shown in Fig. 1. The challenges and perspectives are also provided to enable the reader for an own judgement about the future development of high-performance  $\text{Zn}-\text{CO}_2$  batteries.



Zhihong Tian

Zhihong Tian is a Yellow River Scholar and professor at Henan University. She obtained her first PhD degree in engineering at Zhengzhou University in 2018, and a second PhD degree in natural science at Max Planck Institute of Colloids and Interfaces/Potsdam University in 2019 in Germany. After finishing her PhD studies, she worked as a postdoc in Professor Markus Antonietti's group at Max Planck Institute of Colloids and

Interfaces in Germany. In January 2021, she joined the Engineering Research Center for Nanomaterials at Henan University. Her research interests are the structural design and performance optimization of porous carbon materials.



Tianxi Liu

Dr Tianxi Liu is currently a full professor at the School of Chemical and Material Engineering, Jiangnan University. He received his PhD (1998) from Changchun Institute of Applied Chemistry, Chinese Academy of Sciences, China. His research is mainly engaged in polymer nanocomposites, new energy materials and devices, and nanofibers and their composites.



Table 1 Summary on the components and performance of Zn–CO<sub>2</sub> battery

Catalytic cathodes	Discharge		Power density (mW cm <sup>-2</sup> )	Stability (h)	Catalyst loading (mg cm <sup>-2</sup> )	Energy efficiency (%)	Ref.
	Product	FE (%)					
Metal-free catalysts	CB-NGC-2	CO (g)	80.4	0.51	—	1	—
	C-BN@600	CH <sub>3</sub> OH (l)	50.1	5.42	300	20	57.5
	P@NCA	CO (g)	92	0.8	20	—	36
Non-noble metal catalysts	Fe@NPC	CO (g)	70.1	3	40	1	37
	ZnTe/ZnO@C	HCOOH (l)	68	0.93	36	0.2	38
	Ni <sub>4</sub> N/Ni <sub>3</sub> ZnC <sub>0.7</sub>	CO (g)	68.9	0.85	15	1	39
	Cu-HDA	C <sub>2</sub> products	—	6.48	60	1.5	40
	La <sub>0.5</sub> Sr <sub>0.5</sub> Fe <sub>0.6</sub> MnO <sub>3</sub>	CO (g)	82	1.27	80	2	41
	SnO <sub>2</sub> /MXene	HCOOH (l)	85	4.28	60	1	41.18
	BiC/HCS	HCOOH (l)	92 ± 2	7.2 ± 0.5	65	1	68.9
	PNCB	HCOOH (l)	80	1.43	20	0.96	44
Noble metal-based catalysts	Sn/NCNFs	CO (g)	97.6	1.38	35	1	—
	Ag As/CC	CO (g)	95.3	2.16	50	0.5	45
	Coralloid Au	CO (g)	63	0.7	68	—	47
	BiPdC	HCOOH (l)	52.64	0.42	45	1	48
Single-atom catalysts	Fe-SA/BNC	CO (g)	98.9	1.18	27	1	66.26
	Fe–N <sub>4</sub> O–C/Gr	CO (g)	90.1	0.96	74	0.28	49
	CoPc@DNHCS-8	CO (g)	94	1.02	40	1	50
	Pd1-O-CB	CO (g)	—	1.72	100	0.83	51
	FeNC NSs-1000	CO (g)	90	1.05	30	1	52

## 2 Working principles and devices

Despite the lower energy density than that of the Li–CO<sub>2</sub> battery, the Zn–CO<sub>2</sub> battery has some relevant advantages. It mainly uses aqueous electrolytes without generating solid discharge products, featuring a safer, more environmentally friendly, and greener operation.<sup>54,55</sup> During the discharging process, the Zn foil is oxidized into Zn<sup>2+</sup> at the anode and forms zincate (Zn(OH)<sub>4</sub><sup>2-</sup>) in the alkaline electrolyte, together with the simultaneous occurrence of CO<sub>2</sub>RR at the cathode. During the charging process, Zn<sup>2+</sup> ions are redeposited at the anode, and the OER by water splitting occurs in the current systems at the cathode. The theoretical voltage of the Zn–CO<sub>2</sub> battery is actually lower than that of the Zn–O<sub>2</sub> battery by replacing the oxygen reduction reaction (ORR) with the CO<sub>2</sub>RR,<sup>56</sup> but practically, it might avoid the unchangeable high overpotentials (= energy losses) in the OER while loading the battery. It also simplifies the activation of the otherwise inert ZnO by its electrochemical dissolution with, *e.g.*, formic acid, the potential product of CO<sub>2</sub>-reduction.

We underline here that a more feasible practical Zn–CO<sub>2</sub> battery is presumably better understood as an open asymmetric flow battery: in the deloading phase, CO<sub>2</sub> is filled in for conversion into its reduction products to flow out, while in the loading phase, water has to be added, and oxygen flows out.

In the laboratory evaluation in an H-cell or a thin film battery set-up, we can also focus on the oxidation of formic acid, ethanol, or other liquid reduction products instead of the OER, as they are kept in the cell. Considering that a bipolar membrane (BPM) is generally used as the separator, the products on both sides cannot cross and are not affected by each other (except pH changes). Therefore, analysis of different catalytic cathodes and their selectivity towards

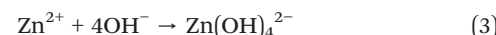
different reaction products is the first step to fix the working mode of a Zn–CO<sub>2</sub> battery during the charging and discharging process. For instance, when CO<sub>2</sub> is reduced to HCOOH during the discharging process, the reactions occur as follows (eqn (1)–(8)):<sup>33</sup>

Cathodic reaction during the discharging process (catholyte: 1 M NaCl, 0.1 M HCOONa, sat. CO<sub>2</sub>):



$$E_c = -0.294 \text{ V}$$

Anodic reaction during the discharging process (anolyte: alkaline electrolyte):



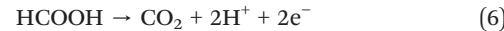
$$E_a = -1.249 \text{ V}$$

Overall reaction of the discharging process:



$$E_{\text{theo}} = 0.955 \text{ V}$$

Cathodic reaction during the charging process:



Anodic reaction during the charging process:



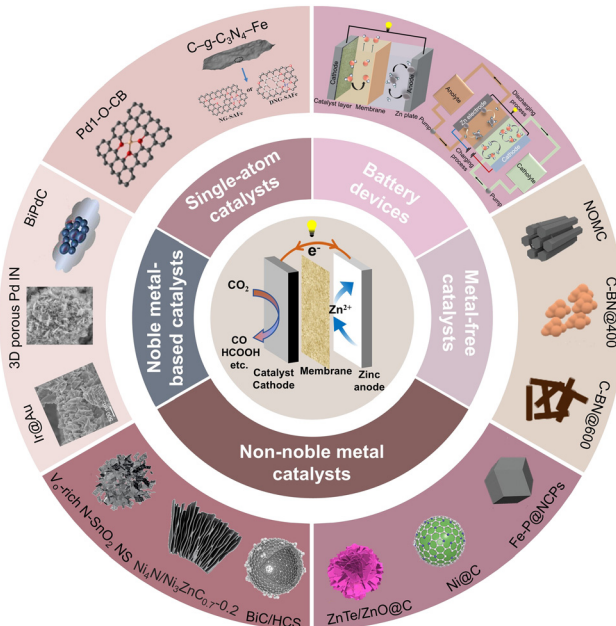
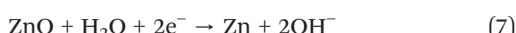
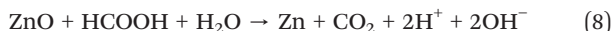


**Fig. 1** A “city-map” of topics and catalysts to develop a future aqueous Zn-CO<sub>2</sub> battery. Reprinted with permission. Reproduced from ref. 29 with permission from WILEY-VCH, copyright 2019. Reproduced from ref. 33 with permission from WILEY-VCH, copyright 2018. Reproduced from ref. 35 with permission from Elsevier, copyright 2023. Reproduced from ref. 38 with permission from American Chemical Society, copyright 2022. Reproduced from ref. 39 with permission from Elsevier, copyright 2022. Reproduced from ref. 43 with permission from Elsevier, copyright 2022. Reproduced from ref. 48 with permission from American Chemical Society, copyright 2022. Reproduced from ref. 52 with permission from Elsevier, copyright 2023. Reproduced from ref. 69 with permission from WILEY-VCH, copyright 2021. Reproduced from ref. 84 with permission from WILEY-VCH, copyright 2023. Reproduced from ref. 88 with permission from WILEY-VCH, copyright 2022. Reproduced from ref. 104 with permission from WILEY-VCH, copyright 2020. Reproduced from ref. 138 with permission from WILEY-VCH, copyright 2020.



Overall reaction of the charging process:



According to these reactions, we see that replacing the oxygen in a metal air battery with the same CO<sub>2</sub> takes some of the theoretical voltage, but simplifies the activation of the otherwise inert ZnO by its electrochemical dissolution in aqueous formic acid. With liquid CO<sub>2</sub> products and avoiding OER contributions, the cell could be run as a classical film battery.

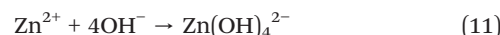
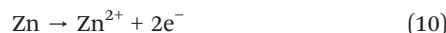
For the reduction of CO<sub>2</sub> into CO as an example of gaseous products during the CO<sub>2</sub>RR, the reaction mechanism is shown in eqn (9)–(18):<sup>29</sup>

Cathodic reaction during the discharging process (catholyte: KHCO<sub>3</sub> sat. CO<sub>2</sub>):



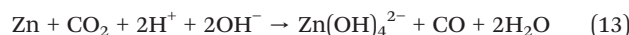
$$E_c = -0.531 \text{ V}$$

Anodic reaction during the discharging process (anolyte: alkaline electrolyte):



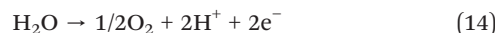
$$E_a = -1.238 \text{ V}$$

Overall reaction of the discharging process:

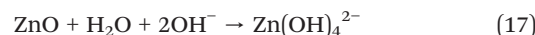


$$E_{\text{theo}} = 0.707 \text{ V}$$

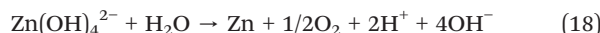
Cathodic reaction during the charging process:



Anodic reaction during the charging process:



Overall reaction of the charging process:



As mentioned above, the OER with sluggish reaction kinetics during the charging process tends to reduce the energy efficiency of the battery. In addition, the high charging voltage can reduce the stability of catalysts. Meanwhile, ZnO can be produced and precipitated in the anodic side during the cycles, which retard the Zn plating/stripping processes and contaminate the electrolyte, resulting in poor cycling performance. Recently, Liu *et al.* have replaced the OER with the oxidation of reducing molecules, which can reduce the charging voltage from 2.45 V to 1.35 V at 4.29 mA cm<sup>-2</sup>. During the charging process, the reducing molecules can be oxidized to N<sub>2</sub>, acetone, or sulfate. This coupling can also effectively improve the stability of catalysts, benefiting the long cycling performance of the battery.<sup>57</sup>

Here, we see that the cell runs in an open fashion: the battery cycle produces CO and oxygen from CO<sub>2</sub> and water, and one part of the invested energy is stored as electricity and the other part is stored as chemical energy: the cell is bifunctional. Ideally, it is then in the hand of the scientists

to run and switch between a “closed” and “open” operation modes, depending on the actual wish to create chemicals or store electricity.

Recent studies have focussed on the design of electrochemical cells and materials due to their key role in improving the performance, including the current density, faradaic efficiency (FE), and stability of the CO<sub>2</sub>RR to a maximal possible extent.<sup>58</sup> Working in an H-cell (Fig. 2a) is the current lab practice for evaluating the catalysts in the Zn–CO<sub>2</sub> battery. The cell is generally divided into an anode chamber and a cathode chamber, which are connected to each other by a connecting channel and separated by ion exchange membranes. At present, the BPM is widely used to maintain the pH due to the different electrolytes used in each channel. The working electrode and reference electrode are placed in the cathode chamber, and the counter electrode is placed in the anode chamber. Such a structure ensures to some extent that the products on both sides are not cross-contaminated during the reaction process, and different electrolytes can be used on both sides. The separation of the different reactions improves the stability of the electrocatalysts. As the mass transfer efficiency in the H-cell is relatively low due to the larger geometric distances involved, the current density achieved in the H-cell is generally far below the requirement of a practical device.

For a real Zn–CO<sub>2</sub> battery targeted for practical applications, an open and asymmetric flow system has to be designed, where CO<sub>2</sub> is continuously filled in and the reductive products flow out; meanwhile, water has to be added due to the consumption for O<sub>2</sub> generation (Fig. 2b). Compared to the widely used H-cell, the flow cell has much smaller distances between the anode and the cathode, which is beneficial for improving transport, minimizing polarization, and thereby improving power density and energy efficiency. Another issue to address in flow batteries is that conditions such as pH and substrate concentrations change along the channel length. For example, the pH around the cathode could be >7 even when the electrolyte is an acid-based solution, originating from the fast reaction kinetics.<sup>59,60</sup> In such cases, the competing HER can be inhibited, while formic acid can be produced instead of

formate, without the necessity of further acidification and distillation. In addition, the battery can run in a nearly constant mode (but at a lower voltage) with the usage of a flowing fluid reservoir. Therefore, further improvements of Zn–CO<sub>2</sub> batteries in terms of energy efficiency and stability are expected by employing flow cells or other specifically designed electrolytic cells.<sup>41,61</sup>

### 3 Catalytic cathodes

As discussed, the electrocatalysts on the cathodes play a very important role in the reaction kinetics and reaction products of the CO<sub>2</sub>RR. In the Zn–CO<sub>2</sub> battery, catalytic cathodes with diverse chemical and electronic structures were applied, which greatly affect the working mechanism, power density, and cycling stability of the battery. We can classify the reported approaches into four types of catalysts: metal-free catalysts, non-noble metal catalysts, noble metal-based catalysts, and single-atom catalysts.

#### 3.1 Metal-free catalysts

Carbon-based materials have been the main metal-free catalysts investigated for the Zn–CO<sub>2</sub> battery due to their good electrical conductivity, large specific surface area, high chemical inertness, and the simplicity to adjust their structure.<sup>62,63</sup> In addition, they are easily available in various forms such as graphenes, carbon nanotubes, or heteroatom-containing carbonized derivatives from organic precursors.<sup>64–66</sup> Normally, pristine carbon materials are electrochemically inert to the CO<sub>2</sub>RR because all the unipolar and only weakly polarizable carbon structures have no clear path to strongly adsorb and activate the CO<sub>2</sub> molecules. Therefore, the electronic structure of C materials has been generally optimized by introducing heteroatoms (e.g., N, B, and P) into the carbon skeleton and constructing carbon defects, which all provide the active sites. It is well analyzed and understood that the doping of heteroatoms increases adsorption enthalpies, reduces the reaction energy barrier of the CO<sub>2</sub>RR, and enhances, for instance, the adsorption of the critical intermediates (e.g., one electron–proton \*COOH) near the active sites.<sup>67,68</sup>

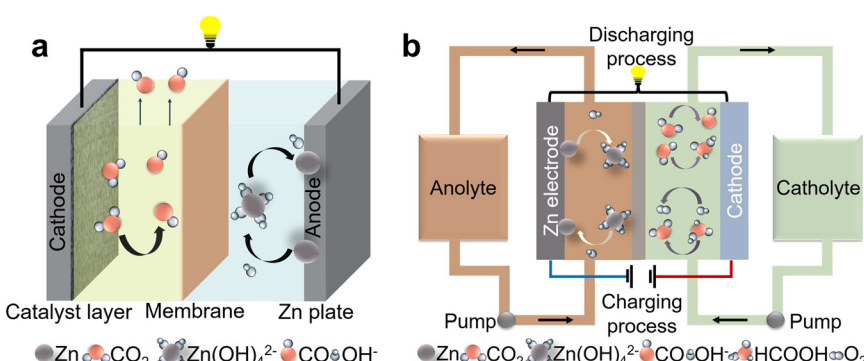


Fig. 2 Schematic diagram of the H-cell (a) and flow cell (b).



For example, Gao *et al.* used the mesoporous silica species SBA-15 as a template to synthesize a nitrogen-doped ordered mesoporous carbon (NOMC), which exhibited abundant parallel channels.<sup>69</sup> The resulting high specific surface area (794.6 m<sup>2</sup> g<sup>-1</sup>) and abundant nitrogen active sites of the NOMC were shown to be beneficial for the transport of reactants during both the CO<sub>2</sub>RR and OER processes. Specifically, the current density of the NOMC (-15.9 mA cm<sup>-2</sup>) was higher than the control samples including ordered regular mesoporous carbon (OMC) (-2.7 mA cm<sup>-2</sup>) and nitrogen-doped carbon (NC) (-2.1 mA cm<sup>-2</sup>) for the CO<sub>2</sub>RR at -0.8 V vs. RHE. Further theoretical calculations suggested that N-doping could significantly reduce the energy barrier required for \*COOH formation, which was considered responsible for the enhanced CO<sub>2</sub>-to-CO activity of the NOMC. In addition, the FE of the NOMC for the CO<sub>2</sub>RR was close to 100% (Fig. 3a) with stable running for 80 h at -0.47 V. Meanwhile, the overpotential of the OER at 10 mA cm<sup>-2</sup> was as low as 586 mV (Fig. 3b), attributed to both the N-doping and exposed surface of the catalyst. The Zn-CO<sub>2</sub>

battery could achieve a peak power density of 0.71 mW cm<sup>-2</sup> and an energy efficiency of 52.8%. Besides, it maintained 76% of FE<sub>CO</sub> at a discharge current density of 1 mA cm<sup>-2</sup> and stable cycling for 300 times. Of course, the FE is relatively low for a real-life battery, but the concept was pioneering.

In addition to the widely studied N, co-doping with other non-metal elements (e.g., B, P, and S) can differently modify the electronic structure by inducing the polarization of carbon near heteroatoms, thereby enhancing the CO<sub>2</sub>RR activity.<sup>35,70,71</sup> For instance, Kaur *et al.* designed and synthesized a B/N-doped carbon with tubular morphology (C-BN@600) as the catalytic cathode for an aqueous Zn-CO<sub>2</sub> battery.<sup>35</sup> The higher surface area of the nanotubular morphology provided more electrochemically active sites, and the presence of heteroatoms B and N improved the mass and charge transport at the electrode-electrolyte interface and thus faster kinetics. As the main adsorption sites, B with insufficient electrons could adsorb the O of CO<sub>2</sub>, while N with a lone pair of electrons binds to C of CO<sub>2</sub>. Compared with N in composite materials, B showed a lower adsorption

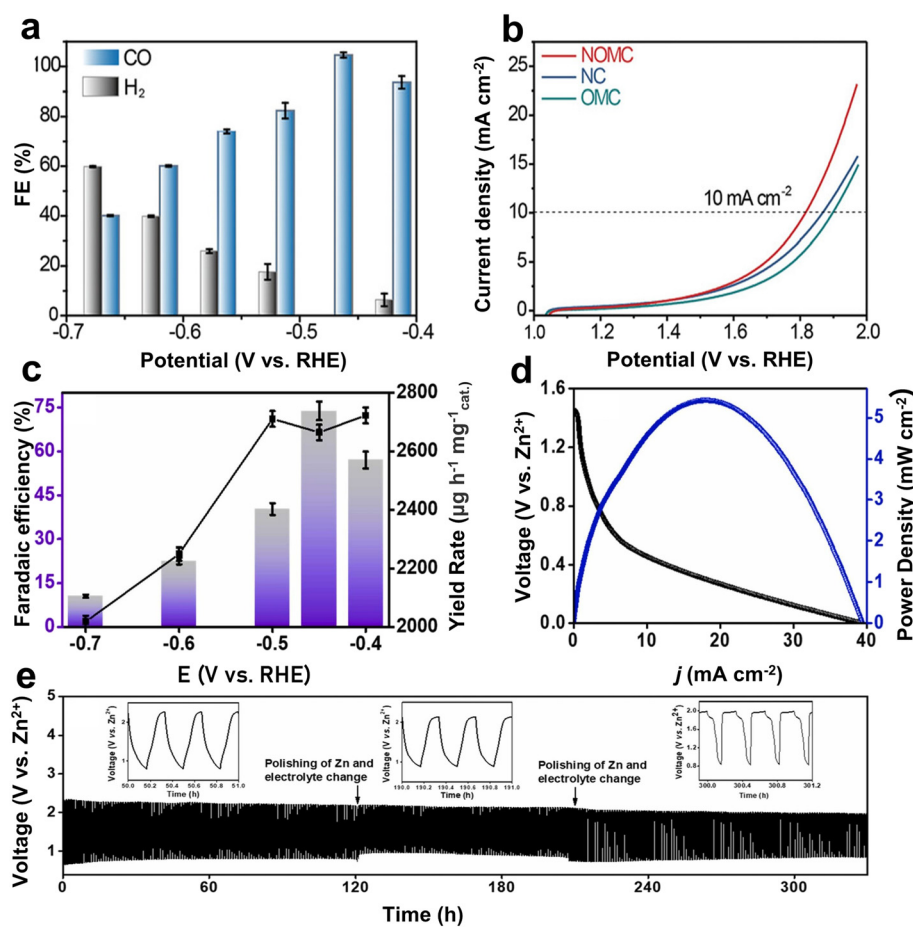


**Fig. 3** (a) FE<sub>CO</sub> in the potentiostatic electrolysis. (b) OER performance evaluated by the linear sweep voltammetry curves of NOMC, OMC, and NC in a 0.8 M KHCO<sub>3</sub> electrolyte with a scan rate of 10 mV s<sup>-1</sup>. Reproduced from ref. 69 with permission from Wiley-VCH, copyright 2021. (c) Bar graph representing the FE and yield rate of CH<sub>3</sub>OH as a product calculated from UV at different potentials. (d) Discharge curve and corresponding power density of the cell at a scan rate of 5 mV s<sup>-1</sup>. (e) Galvanostatic charge-discharge cycles at 1 mA cm<sup>-2</sup>. Reproduced from ref. 35 with permission from Elsevier, copyright 2023.



free energy for the intermediates  $^*\text{COOH}$  and  $^*\text{CO}$ . The better  $\text{CO}_2\text{RR}$  electrocatalytic ability of C-BN@600 was reflected in a more positive onset potential and larger current density. Meanwhile, the synergistic effect of B/N promoted the effective adsorption of intermediates and accelerated the electron transfer to liberate  $\text{CH}_3\text{OH}$  with an FE of 74% (Fig. 3c). The assembled Zn– $\text{CO}_2$  battery exhibited a power density of  $5.42 \text{ mW cm}^{-2}$  and enabled stable cycling for more than 300 h (Fig. 3d and e).

### 3.2 Non-noble metal catalysts

Although the metal-free catalysts are widely studied with the merits of low cost, chemical inertness, and good conductivity, their catalytic performance is fundamentally limited due to the active sites only based on covalent chemistry. Non-noble metals (e.g., Fe, Co, and Ni) are good choices, as they are

easily available, with abundant active sites, and have been demonstrated to show good catalytic activity and high selectivity.<sup>72–75</sup> In particular, supporting non-noble metal species with carbon-based materials can maintain good dispersion of metals and reduces the agglomeration of high surface area species.<sup>76,77</sup> Adjusting the carbon skeleton can also change the electron density in the metal center and improve the electrochemical performance of the composite material.<sup>78,79</sup>

Metal–organic frameworks (MOFs) have attracted attention as precursors of non-noble metal-based catalysts due to their ordered structural morphology and unique coordinative sites.<sup>80</sup> After carbonization, heteroatom-doped metal/carbon composites can be obtained with high porosity, high specific surface area, and tunable pore size.<sup>81–83</sup> Teng *et al.* prepared a ZnTe-MOF-derived ZnTe/ZnO@C (Fig. 4a) as the electrocatalyst, which showed a selectivity of 83% towards

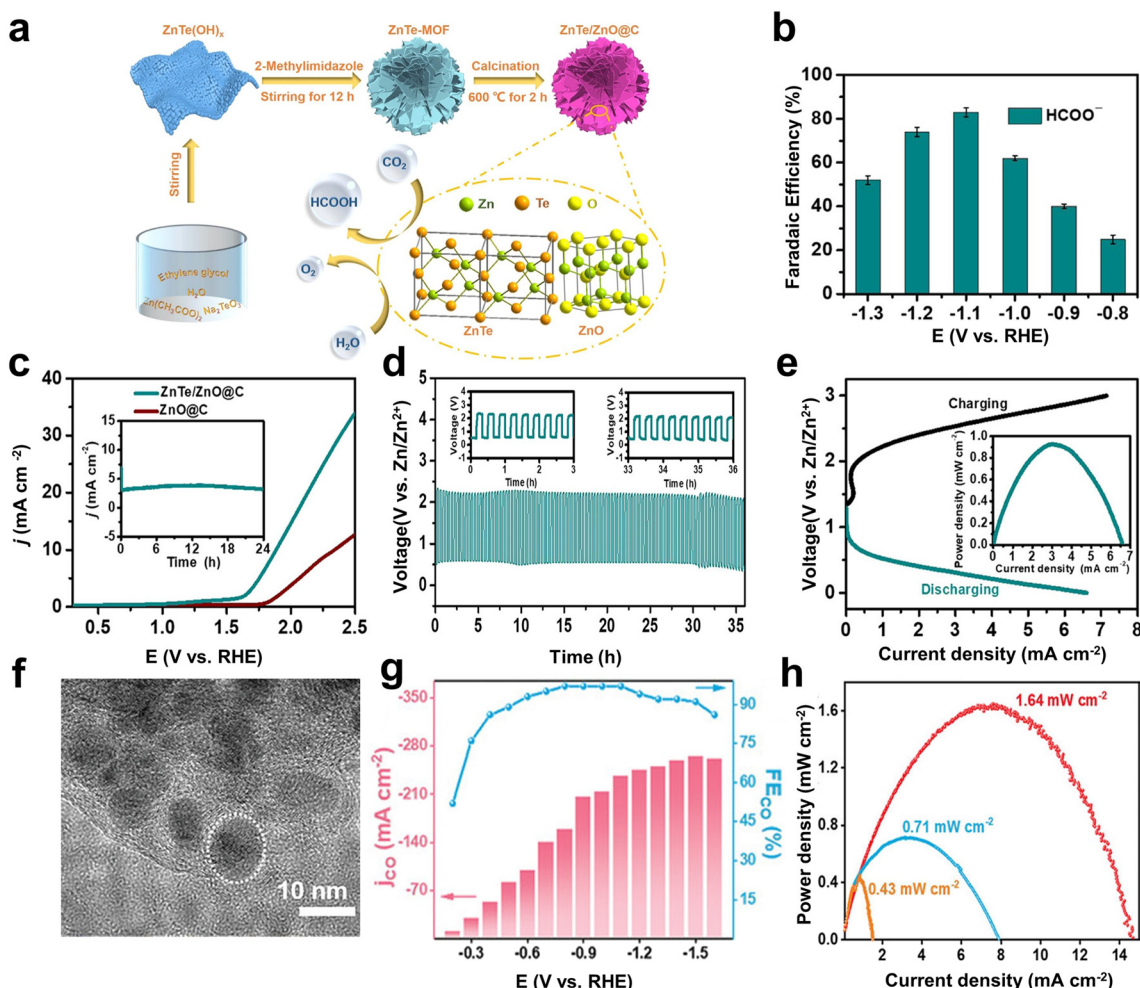


**Fig. 4** (a) Schematic illustration for the preparation of  $\text{ZnTe/ZnO@C}$  as a bifunctional electrocatalyst for the selective  $\text{CO}_2$  reduction coupled with the OER. (b) Variations in  $\text{FE}_{\text{HCOO}^-}$  with potentials. (c) LSV curves for the OER for  $\text{ZnTe/ZnO@C}$  and  $\text{ZnO@C}$  electrodes in 0.5 M  $\text{KHCO}_3$ . The inset shows the results of OER stability measurements on  $\text{ZnTe/ZnO@C}$  for a period of 24 h at 1.7 V. (d) Galvanostatic discharge–charge curves at 1  $\text{mA cm}^{-2}$  for 108 cycles over 36 h. (e) Charge–discharge polarization curves for a Zn– $\text{CO}_2$  battery. The curve in the inset shows the power density at different current densities. Reproduced from ref. 38 with permission from American Chemical Society, copyright 2022. (f) High-resolution TEM (HRTEM) image of Ni@N-C. (g)  $\text{FE}_{\text{CO}^-}$  and  $\text{J}_{\text{CO}}$  with different applied potentials of Ni@N-C in the flow cell. (h) Power density curves of Zn– $\text{CO}_2$  battery. Reproduced from ref. 84 with permission from Wiley–VCH, copyright 2023.



formate at  $-1.1$  V (vs. RHE) (Fig. 4b).<sup>38</sup> The high performance was attributed by the authors to the special flower-like structure of ZnTe/ZnO@C, which could provide abundant active sites. Further theoretical calculations revealed that the synergistic effect between ZnTe sites and ZnO was also conducive to the performance improvement. In particular, ZnTe(111) was favorable to the first step of proton-coupled electron transfer and easily adsorbed the \*OCHO intermediate ( $-1.55$  eV), and the subsequent proton-coupled electron transfer to form \*HCOOH occurred on ZnO(100). Meanwhile, ZnTe/ZnO@C also had good catalytic performance for OER in the neutral carbonate solution ( $10$  mA cm $^{-2}$  at  $1.9$  V) (Fig. 4c). After being assembled into a Zn-CO $_2$  battery, the battery exhibited stability for  $36$  h and a peak power density of  $0.93$  mW cm $^{-2}$  (Fig. 4d and e). Actually, a typical, obvious hysteresis between loading and de-loading curves can be observed (Fig. 4e), indicating that a potential battery use is inhibited by high polarization and suboptimal kinetics. Hence, the peak power density is much lower than that of practical batteries, including lithium-ion batteries. The presented concept of a Zn-CO $_2$  battery is interesting

from an academic view, but needs engineering developments towards a real battery application.

In addition, Wang *et al.* used SBA-15 as a template to prepare nickel-based metal-organic frameworks (Ni-MOFs), giving finally Ni nanoparticles encapsulated in N-doped carbon shells (Ni@N-C) *via* pyrolysis and etching (Fig. 4f).<sup>84</sup> The doping of N could adjust the local electronic structure in the carbon shell, enabling the stronger CO $_2$  adsorption, faster electron transfer rate, and more exposed active sites in synergy with metallic Ni. As revealed by the theoretical calculations, the Fcc-Ni@N-C had weak van der Waals interaction between N-C and metallic Ni and tended to evolve into more stable Top-Ni@N-C after the adsorption of CO $_2$ . The other model of Hcp-Ni@N-C had a large thermodynamic barrier in the step of CO $_2$  adsorption, because the CO $_2$  bonding to one N atom caused the breaking of one N-Ni bond. Therefore, the most thermodynamically stable configuration was N-C located on the top of Ni slabs (Top-Ni@N-C), which had the lowest thermodynamic barrier to the formation of \*COOH and the desorption of CO. As a result, Ni@N-C exhibited a large current density of  $244$  mA

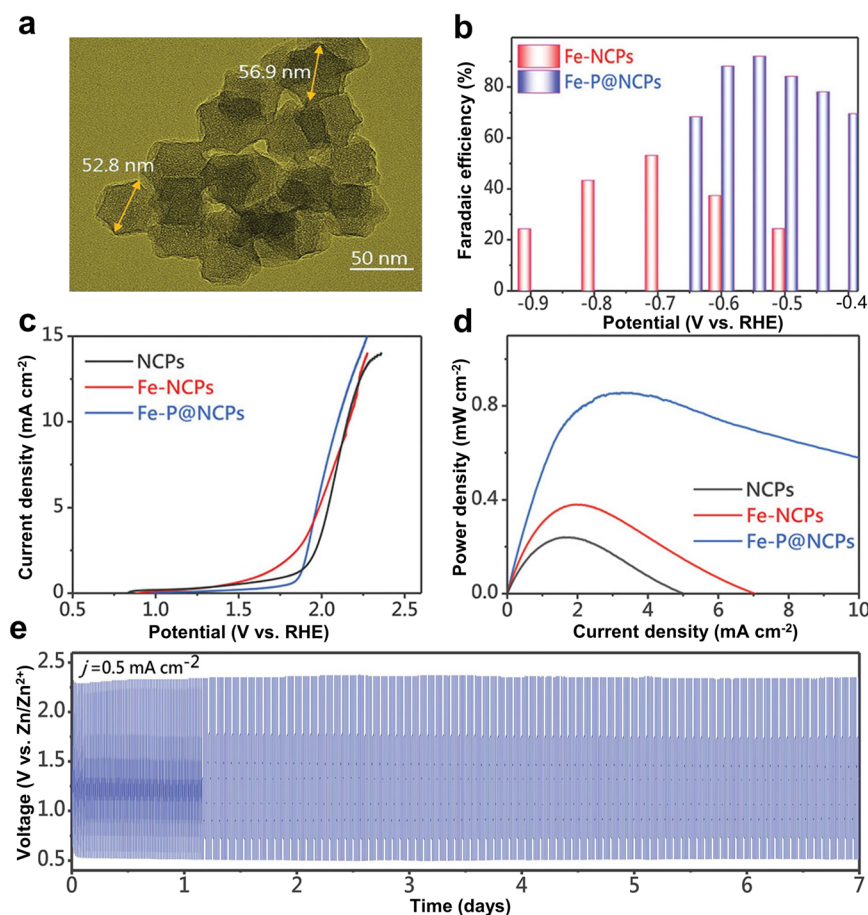


Fig. 5 (a) TEM image of the synthesized Fe-P@NCPs. (b) FE<sub>CO</sub> values at different applied potentials for Fe-NCPs and Fe-P@NCPs. (c) OER evaluation by the LSV curves in a  $0.1$  M KHCO $_3$  solution. (d) Power density curves of the aqueous Zn-CO $_2$  cell based on different samples. (e) Galvanostatic discharge-charge cycling curves at  $0.5$  mA cm $^{-2}$  for Fe-P@NCPs. Reproduced from ref. 88 with permission from Wiley-VCH, copyright 2022.



cm<sup>-2</sup> and a high FE<sub>CO</sub> of 97% at -1.1 V (vs. RHE) in the flow cell (Fig. 4g). As the catalytic cathode for the Zn-CO<sub>2</sub> battery, a maximum power density of 1.64 mW cm<sup>-2</sup> and a cycling performance of 45 h were achieved (Fig. 4h).

Compared to N coordination, the P atom has a multi-electron p orbital and relatively weak electronegativity, providing additional properties in tuning the electronic structure of substrates.<sup>85-87</sup> Liu *et al.* introduced Fe-P nanocrystals into N-doped carbon polyhedrons (Fe-P@NCPs) (Fig. 5a).<sup>88</sup> Compared with N-doped carbon polyhedrons (NCPs), the Fe-N doped carbon polyhedrons (Fe-NCPs) and Fe-P@NCPs showed better CO<sub>2</sub>RR performance. These results indicated that Fe-N and Fe-P active sites could play important roles toward the CO<sub>2</sub>RR. As mentioned above, the P atom had relatively weak electronegativity, allowing electrons to transfer less against a diodic surface potential. As a result, the Fe-P unit, as the activation center of CO<sub>2</sub>, could easily transfer more electrons for CO<sub>2</sub> reduction. As a result, Fe-P@NCPs showed a higher CO selectivity (FE<sub>CO</sub> =

95%) (Fig. 5b). In addition, Fe-P@NCPs showed an overpotential of 840 mV at 10 mA cm<sup>-2</sup> for the OER in aqueous KHCO<sub>3</sub> (0.1 M) as the electrolyte (Fig. 5c). The Zn-CO<sub>2</sub> battery (referred to H-cell) with the Fe-P@NCP cathode showed a peak power density of 0.85 mW cm<sup>-2</sup> but maintained outstanding stability over 7 days without degradation (Fig. 5d and e). It has to be mentioned that the alkaline electrolyte in the H-cell will dominantly react and buffer with CO<sub>2</sub>. Therefore, the flow cell coupled with a gas diffusion electrode, which can employ the alkaline electrolyte, is a desirable configuration for the Zn-CO<sub>2</sub> battery.

It has also been reported that introducing solar energy into an electrochemical device (e.g., Li-CO<sub>2</sub>, Li-O<sub>2</sub>, Zn-air) can improve the energy efficiency and reaction kinetics of the CO<sub>2</sub>RR and ORR.<sup>89-92</sup> Liu *et al.* developed an ultra-thin Cu<sub>2</sub>O/CuCoCr-LDH (layered double hydroxide) photocathode.<sup>93</sup> Benefiting from the ultra-thin p-n heterojunction nanosheets on the photocathode, it could not only effectively separate

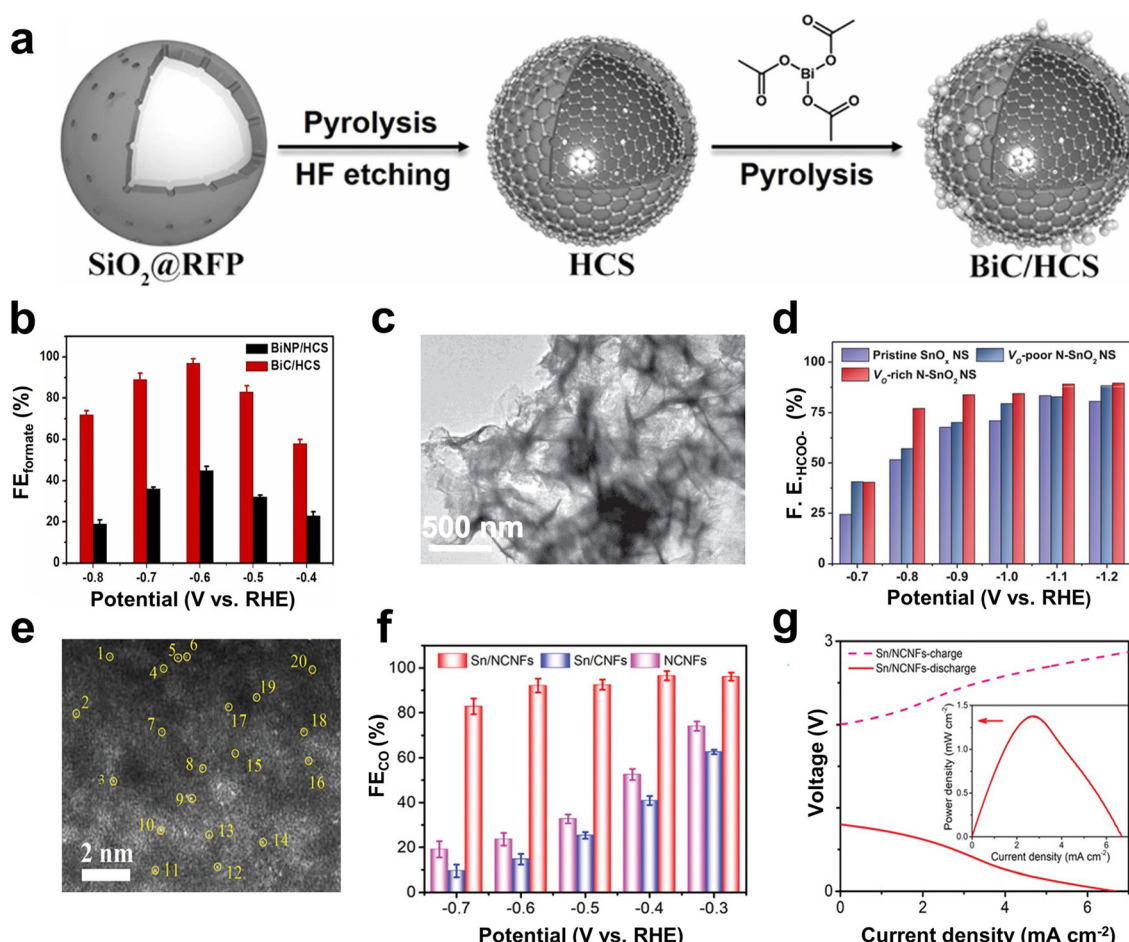


**Fig. 6** (a) Schematic illustration of the synthesis procedure. (b) FE<sub>formate</sub> values at different applied potentials. Reproduced from ref. 43 with permission from Elsevier, copyright 2022. (c) TEM images of the V<sub>O</sub>-rich N-SnO<sub>2</sub> NS. (d) FE<sub>HCOO<sup>-</sup></sub> of the pristine SnO<sub>x</sub> NS, the V<sub>O</sub>-poor N-SnO<sub>2</sub> NS and V<sub>O</sub>-rich N-SnO<sub>2</sub> NS at different potentials. Reproduced from ref. 104 with permission from Wiley-VCH, copyright 2020. (e) HAADF-STEM image of Sn/NCNFs with atomic-level Sn atoms highlighted by yellow circles. (f) FE<sub>CO</sub> of Sn/NCNFs, Sn/CNFs, and NCNFs at different potentials in a flow cell. (g) Polarization curves and power density (inset) of Sn/NCNFs. Reproduced from ref. 45 with permission from Wiley-VCH, copyright 2022.



photogenerated electrons and holes and promote electron transfer, but also provide abundant  $\text{CO}_2$  adsorption and reaction sites. As a result, the  $\text{Cu}_2\text{O}/\text{CuCoCr-LDH}$  showed a good selectivity (FE = 90.14%) and a yield of  $1167.6 \mu\text{mol g}^{-1} \text{h}^{-1}$  towards CO. As the cathode of a model Zn– $\text{CO}_2$  battery under light, the battery had a discharge voltage of 1.22 V (higher than the discharge voltage of a light-free Zn– $\text{CO}_2$  battery of 0.59 V), and exhibited good cycling stability within 54 h.

Bi-based catalysts have demonstrated good adsorption properties for  $^*\text{OCHO}$  intermediates, and thus, can selectively catalyze the reduction of  $\text{CO}_2$  to formate.<sup>94–96</sup> The  $^*\text{OCHO}$  intermediate can be stabilized by regulating the electron accumulation of Bi nanoparticles by supports containing pyrrolic-N. Besides, benefitting from the combined effect of special structural design and good conductivity, the catalyst exhibits faster reaction kinetics and high formate formation rate.<sup>44</sup> For example, Yang *et al.* demonstrated that Bi clusters dispersed on the hollow carbon spheres (BiC/HCS) (Fig. 6a) could stabilize the  $^*\text{OCHO}$  intermediate, which can facilitate the  $\text{CO}_2\text{RR}$  to form formate and inhibit the competitive HER as well.<sup>43</sup> The maximum FE<sub>formate</sub> at  $-0.6$  V (vs. RHE) was  $97 \pm 2\%$  (Fig. 6b). The Zn– $\text{CO}_2$  battery based on the BiC/HCS cathode showed a peak power of  $7.2 \pm 0.5 \text{ mW cm}^{-2}$  and a cycling performance of 200 times. In addition, the introduction of other metals (such as Cu, Ti, and In) into Bi-based materials enhanced the adsorption of  $^*\text{OCHO}$  intermediates and improved the FE of formic acid.<sup>97–99</sup> For instance, a Bi/In bimetal catalyst turned out to be favorable for producing the key intermediate  $^*\text{OCHO}$  from  $\text{CO}_2$  to formate, and synergistically reduced the free energy from  $^*\text{OCHO}$  to  $^*\text{HCOOH}$ , thereby promoting the production of  $\text{HCOOH}$ .<sup>99</sup>

In addition, In- and Sn-based metal catalysts have been proven to have good selectivity towards formate.<sup>100–102</sup> Teng *et al.* designed an In/ZnO@C hollow nanocube electrocatalyst.<sup>103</sup> Through *in situ* doping, In could be evenly distributed on the cube, and the hollow cube structure provided more exposed active sites. Therefore, In/ZnO@C exhibited a good catalytic activity and formic acid selectivity. At  $-1.2$  V (vs. RHE), the partial current density for formate production reached  $23.5 \text{ mA cm}^{-2}$  with an FE of 90%. As an electrocatalytic cathode for the aqueous rechargeable Zn– $\text{CO}_2$  battery, the battery reached a power density of  $1.32 \text{ mW cm}^{-2}$  and was cycled for 51 h at a current density of  $1 \text{ mA cm}^{-2}$ . Li *et al.* prepared N-doped  $\text{SnO}_2$  nanosheets with oxygen vacancies ( $\text{V}_\text{O}$ -rich N- $\text{SnO}_2$  NS) (Fig. 6c).<sup>104</sup> The electronic junction and geometric structure of  $\text{SnO}_2$  were adjusted *via* N doping and  $\text{V}_\text{O}$ , which was expected to be beneficial for the protonation pathway of  $^*\text{OCHO}$  while inhibiting the adsorption of  $^*\text{H}$  on the  $\text{SnO}_2$  surface. At a potential of  $-0.9$  V,  $\text{V}_\text{O}$ -rich N- $\text{SnO}_2$  NS exhibited good  $\text{CO}_2\text{RR}$  performance, and the FE of  $\text{HCOO}^-$  was about 83% (Fig. 6d). However, by regulating the electronic structure of the active site, the binding energy of the active center Sn to  $^*\text{OCHO}$  and  $^*\text{COOH}$  intermediates could be changed, which in turn changed the

$\text{CO}_2\text{RR}$  product.<sup>105</sup> Hu *et al.* demonstrated that Sn–N as the active site in porous N-doped carbon nanofibers (Sn/NCNFs) (Fig. 6e) accelerated the dissociation and proton transfer of  $\text{H}_2\text{O}$ , thereby promoting the formation of  $^*\text{COOH}$  intermediates.<sup>45</sup> Meanwhile, the pyrrolic N adjacent to the Sn–N active site helped to reduce the formation energy barrier of the  $^*\text{COOH}$  intermediate, thereby improving the kinetics of the  $\text{CO}_2\text{RR}$ . As a result, Sn/NCNFs exhibited a high  $\text{CO}_2\text{RR}$  activity, and the FE of CO was as high as 96.5% (Fig. 6f). The peak power density of the Zn– $\text{CO}_2$  battery with Sn/NCNFs as the cathode reached  $1.38 \text{ mW cm}^{-2}$  (Fig. 6g).

### 3.3 Noble metal-based catalysts

Despite scarcity and high cost, noble metal catalysts are still widely used in the field of electrochemistry due to their excellent catalytic activity, high stability and high selectivity.<sup>106–108</sup> In this field, it is a challenge to use less noble metals for the same reactivity. For that, it has been demonstrated that the catalytic performance of noble metal catalysts can be optimized through crystal facet control and nanostructure engineering.<sup>109–113</sup> In addition, strategies such as alloying other metals or loading on conductive substrates are used to leverage the catalytic performance of precious metals while reducing costs.<sup>114,115</sup> Currently, noble metal catalysts including Pd, Au, and Ag are still typical choices for the aqueous Zn– $\text{CO}_2$  battery.<sup>46,48,116</sup>

Pd catalysts can not only reduce  $\text{CO}_2$  to  $\text{HCOOH}$ , but also oxidize  $\text{HCOOH}$  to  $\text{CO}_2$ .<sup>117,118</sup> Therefore, Pd-based catalysts are suitable as bifunctional catalytic cathodes for the Zn– $\text{CO}_2$  battery. In 2018, Xie *et al.* proposed and prepared a reversible Zn– $\text{CO}_2$  battery for the first time (Fig. 7a).<sup>33</sup> The battery used Pd nanosheets as the bifunctional catalytic cathode (Fig. 7b) and realized reversible conversion between  $\text{CO}_2$  and  $\text{HCOOH}$  during the discharging and the charging process. In order to obtain good catalytic performance for the  $\text{CO}_2\text{RR}$  and the oxidation of formic acid (FAO), respectively, the morphology and structure of Pd-based catalysts were carefully modified. The experimental results showed that Pd nanosheets rich in edges and pores promoted the  $\text{CO}_2\text{RR}$  towards  $\text{HCOOH}$  with an FE of 90% (partial current density was  $15 \text{ mA cm}^{-2}$ ) (Fig. 7c). Moreover, FAO could produce a stable current of  $4.3 \text{ mA cm}^{-2}$  at a voltage of  $0.3$  V, and gas chromatography proved that the product was  $\text{CO}_2$ . A Zn– $\text{CO}_2$  battery based on Pd nanosheets as the cathode showed an energy efficiency of 81.2% and a cycling durability of more than 100 cycles.

To explore bi-functional noble metal-based catalytic cathodes for Zn– $\text{CO}_2$  batteries, Wang *et al.* prepared Ir@Au bimetallic nanomaterials by combining chemical deposition and electrochemical deposition (Fig. 7d).<sup>29</sup> In particular, it was found that pristine Ir showed a higher partial current density of HER than that of Ir@Au and Au, while the partial current density to CO was significantly lower than that of the other two samples (Fig. 7e). In comparison, the partial current density of CO from pure Au was slightly higher than that of Ir@Au. Therefore, the results showed that the



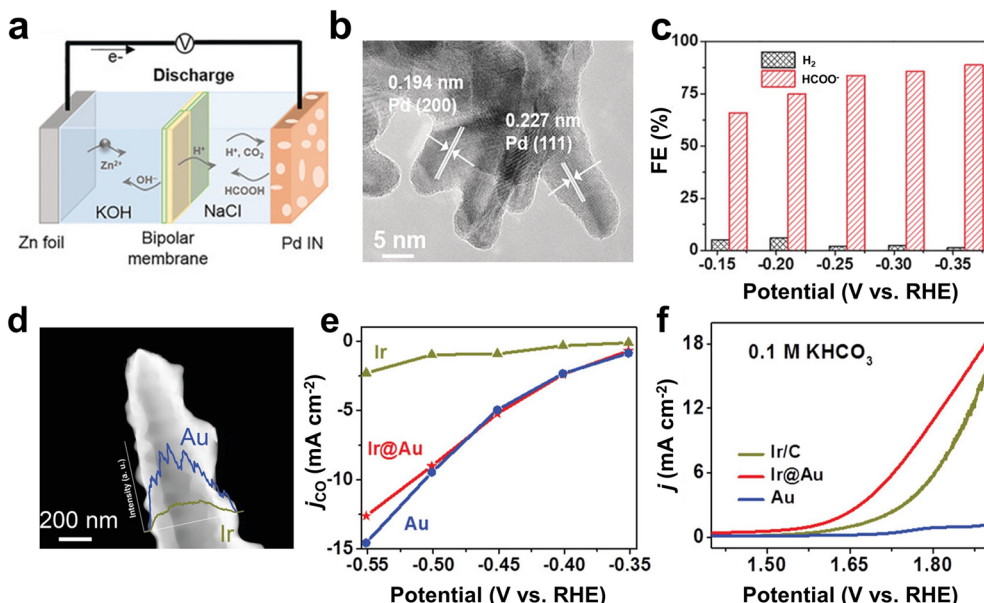


**Fig. 7** (a) Schematic of the reversible aqueous Zn–CO<sub>2</sub> battery. (b) HRTEM image of the as-prepared Pd nanosheet. (c) FE of different products at various potentials. Reproduced from ref. 33 with permission from Wiley-VCH, copyright 2018. (d) HAADF image and corresponding linear elemental mapping of gold and iridium. (e) Partial current density of CO ( $j_{CO}$ ) in potentiostatic electrolysis. (f) OER performance evaluated by the LSV curves. Reproduced from ref. 29 with permission from WILEY-VCH, copyright 2019.

introduction of Au could inhibit the occurrence of HER in Ir@Au and generate a higher selectivity of Au for CO. In addition, Ir@Au performed comparably to Ir/C catalysts as a commercial OER catalyst. Accordingly, the Ir@Au bimetallic nanomaterial exhibited a pleasing selectivity for CO ( $-0.5$  V, FE  $\approx 85\%$ ) and good OER performance with a current density of  $10$  mA cm<sup>-2</sup> at  $1.79$  V (Fig. 7f). As a catalytic cathode of Zn–CO<sub>2</sub>, the battery had an energy efficiency of  $68\%$  and a cycling stability of  $30$  h. It is however clear that Ir is a very rare element and thereby not favorable for large-scale practical applications.

#### 3.4 Single-atom catalysts

Single-atom catalysts (SACs) have received great attention due to their atom efficiency, as well as their unique catalytic properties. Compared to the nanoparticle-based catalysts, the single-atom metal active sites distributed on a conductive substrate can achieve maximum atomic utilization.<sup>119–121</sup> Importantly, the catalytic activity and selectivity in a specific metal atom can be fine-tuned in a wider range through its coordination environment.<sup>122–125</sup> Usually, metals are introduced into heteroatom-doped carbon materials by methods such as pyrolysis and electrochemical deposition to adjust the electronic structure of the active center, thereby modifying the CO<sub>2</sub>RR and OER performance of the catalyst.<sup>126–128</sup>

For example, Li *et al.* constructed N- and O-coordinated single-atom Pd catalysts (Pd1-N-CB and Pd1-O-CB, respectively).<sup>52</sup> The results showed that the asymmetric coordination and strong regulation of O to the Pd center

enabled Pd1-O-CB to show excellent CO<sub>2</sub>RR selectivity for CO at lower potentials ( $99.6\%$  under  $-0.6$  V vs. RHE). The theoretical calculations further proved that the O-coordinated Pd1-O-CB provided more electrons than the N-coordinated Pd1-N-CB to the \*COOH intermediate, and thus achieved the lowest free energy of the potential-determining step (PDS) ( $\Delta G = 1.02$  eV). In addition, the desorption of \*CO on Pd1-O-CB was easier than that of Pd nanoparticles, preventing CO product inhibition of Pd active sites. As the cathode of a Zn–CO<sub>2</sub> battery, the Pd1-O-CB cathode showed a power density of  $1.72$  mW cm<sup>-2</sup> and an endurance of at least  $100$  h for CO production.

Currently, the metal/N-doped carbon (M–N–C) is a widely studied class of electrocatalysts. The doping with N can reduce the formation energy of CO<sub>2</sub>RR intermediates such as \*COOH and \*OCHO on the M–N active site, thus showing higher selectivity.<sup>129–131</sup> Compared with noble metals, single-atom catalysts of transition metals such as Fe, Co, and Ni have more economic benefits.<sup>132–135</sup> For example, Gong *et al.* anchored cobalt phthalocyanine on N-doped hollow carbon spheres with carbon defects (CoPc@DNHCS-8) (Fig. 8a).<sup>51</sup> The N-doping strategy provided the electron-withdrawing effect of the carbon matrix, resulting in the formation of Co(II) sites. Under cathodic bias, Co(II) could obtain electrons and be reduced to Co(I), which was generally considered to be the catalytic active site for CO<sub>2</sub> reduction. The CO<sub>2</sub> could gain electrons and be activated at the Co(I) site to form the intermediate \*COOH (Fig. 8b). As a result, CoPc@DNHCS-8 showed a high FE<sub>CO</sub> of  $95.68\%$ . The Zn–CO<sub>2</sub> battery based on CoPc@DNHCS-8 exhibited a maximum power density of  $1.02$  mW cm<sup>-2</sup> and a cycling stability of  $40$  h (Fig. 8c).

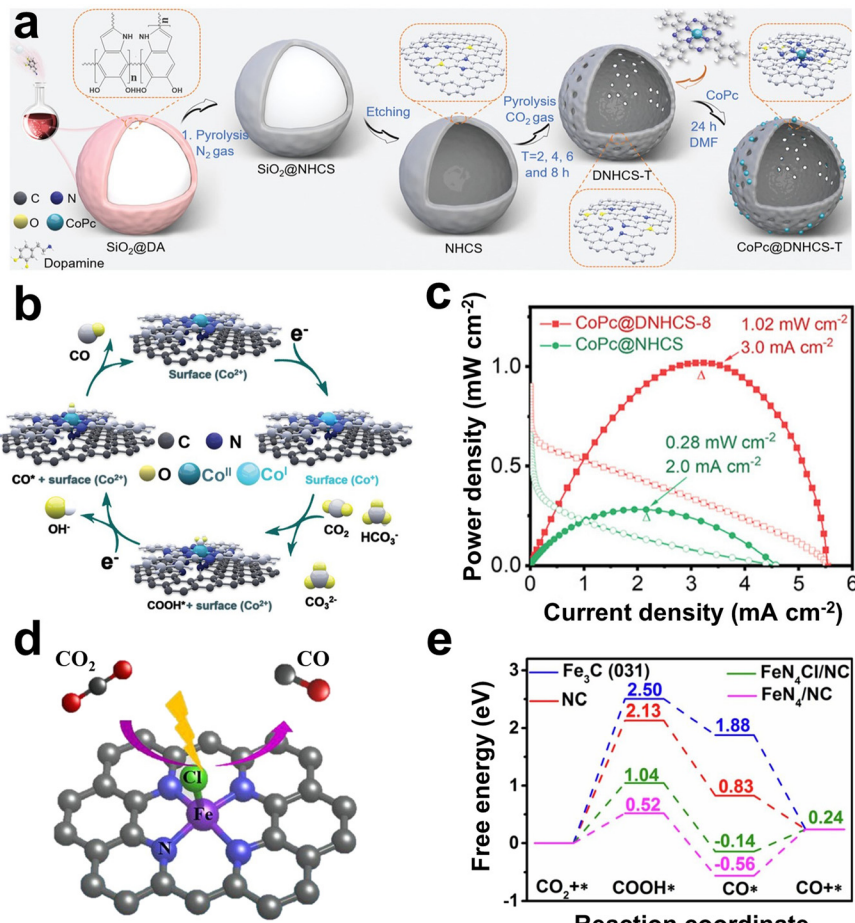


**Fig. 8** (a) Scheme of the formation of CoPc@DNHCS-T series ( $T = 2-8$ ). (b) Mechanism model diagram of CO<sub>2</sub>-to-CO reaction pathway. (c) Power density curves of the Zn-CO<sub>2</sub> battery based on CoPc@DNHCS-8 and CoPc@NHCS as the cathode. Reproduced from ref. 51 with permission from Wiley-VCH, copyright 2022. (d) Schematic structural model of FeN<sub>4</sub>Cl/NC. (e) Free-energy profiles of reaction intermediates in the CO<sub>2</sub>RR on different catalysts. Reproduced from ref. 134 with permission from Elsevier, copyright 2021.

Single-atom Fe-based catalysts are another promising choice, due to the abundance of iron and its low onset potential in the CO<sub>2</sub>RR.<sup>136,137</sup> However, some studies have proven that in the coordination form of Fe-N<sub>4</sub>, the active sites are inhibited due to the strong adsorption of \*CO intermediates.<sup>138-140</sup> Ni *et al.* found that the true active sites for CO<sub>2</sub> reduction were associated with intrinsic defects rather than the Fe-N<sub>4</sub> centers. Further calculations showed that these defects, coupled with Fe-N<sub>4</sub>, demonstrated a diminished energy barrier for CO<sub>2</sub> reduction and concurrently mitigated hydrogen evolution activity.<sup>138</sup> In addition to the N atoms, other types of heteroatoms such as Cl, B, P, and O are often used to coordinate with single metal atoms.<sup>49,50,134</sup> For example, Li *et al.* adjusted the electronic structure of Fe in Fe-N<sub>4</sub> by introducing an axial chlorine (Cl) ligand (Fig. 8d), thereby promoting the desorption of \*CO and inhibiting the adsorption of \*H.<sup>134</sup> Further DFT calculations showed that the formation energy barrier of \*COOH on FeN<sub>4</sub>Cl in N-doped carbon (FeN<sub>4</sub>Cl/NC) (1.04 eV) was lower than that on NC (2.13 eV) and Fe<sub>3</sub>C (2.50 eV), but higher than that on Fe-N<sub>4</sub>/NC (0.52 eV) (Fig. 8e). Besides,

desorption of \*CO to CO had a lower energy barrier on FeN<sub>4</sub>-Cl/NC (0.38 eV) than that on Fe-N<sub>4</sub>/NC (0.80 eV). In addition, the adsorption energy of \*H on FeN<sub>4</sub>Cl/NC was higher than that of Fe-N<sub>4</sub>/NC and Fe<sub>3</sub>C, indicating that the introduction of Cl atoms inhibited HER. Therefore, FeN<sub>4</sub>Cl/NC exhibited excellent CO<sub>2</sub>RR performance, showing a high FE<sub>CO</sub> of 90.5% at a promising current density of 10.8 mA cm<sup>-2</sup> with an overpotential of 490 mV. As the cathode of an aqueous Zn-CO<sub>2</sub> battery, the battery showed a power density of 0.545 mW cm<sup>-2</sup> and a cycling stability of 15 h.

## 4 Summary and outlook

Overall, we reviewed a very interesting collection of current studies which indicate the high potential of aqueous Zn-CO<sub>2</sub> batteries as a green and sustainable energy storage and conversion technology. The use of compressed CO<sub>2</sub> saves more, showing better solubility in aqueous solvents, than the current Zn-O<sub>2</sub> battery (which is very difficult to cycle effectively), and it conceptually avoids the high overpotentials and, thereby, energy losses of ORR and OER. In addition,

$\text{CO}_2$  reduction products such as formic acid promote the redissolution of  $\text{ZnO}$ , thereby improving the cyclability. The battery however can also be run in an asymmetric open flow mode, thus combining energy storage with the electrochemical production of  $\text{CO}_2$ -based chemicals in discharging while oxidizing water to  $\text{O}_2$  in the charging process. This disruptive concept that combines  $\text{CO}_2$  conversion and energy supply comes with the disadvantage of losing energy in the OER again while being flexible to switch between electricity and chemical generation, depending on the actual demand.

As the Zn-metal anode is well understood and the state of the art, research efforts mainly focus on the development of efficient electrocatalytic (flow) cathodes. In view of the different redox reactions of the Zn- $\text{CO}_2$  battery during the charging and discharging processes, the electrocatalytic cathode needs to be able to simultaneously promote the  $\text{CO}_2$ -RR to defined products while suppressing the HER as the competing, here parasitic reaction. For this purpose, traditional noble metal-based catalysts (Pd, Ag, *etc.*), but more scalable, also metal-free carbon-based material catalysts, non-noble metal catalysts, and supported single-atom catalysts were developed as potential cathode materials for a potential Zn- $\text{CO}_2$  battery.

However, the research on aqueous Zn- $\text{CO}_2$  batteries is still in its infancy, and a number of questions should be addressed. First, the catalytic cathodes determine whether the  $\text{CO}_2$ -RR product during the discharging process is a gas-phase or liquid-phase product.  $\text{C}=\text{O}$  is, in the consumer space, a critical product which comes with safety measures, but higher-value reduction products such as methanol also come with a higher energy storage density (6 electrons instead of only 2). A liquid-phase product could be oxidized to regenerate  $\text{CO}_2$ , enabling a closed battery system. In an open, switchable system, the reaction that occurs at the cathode during the charging process is the OER, and at the anode, it is the redeposition of  $\text{Zn}^{2+}$ . The catalytic performance of the electrocatalyst for the OER will critically affect the energy efficiency of the overall system.

Second, most of the current research studies are conducted with H-cells, and the voltage hysteresis between loadings is correspondingly high, mostly due to the polarization issues and long charge transport distances involved. Going to a real, flat and thin battery geometry comes with extra problems, which however should be tackled before calling such systems “batteries”. One of the problems is the limited solubility of  $\text{CO}_2$  in aqueous electrolytes, which is not an issue in high-solvent volume H-cells, but requests either a three-phase boundary gas electrode or a flow cell geometry for the practical solutions. Improving the solubility of  $\text{CO}_2$  in electrolytes and/or pressurized cells (“soda cells”) could also be a focus for future experiments. As it is still unclear whether dissolved  $\text{CO}_2$  or  $\text{HCO}_3^-$  in the electrolyte operates as the carbon source in the discharging process, further research might consider investigating the underlying mechanisms by providing the specific carbon sources. This would extend the

engineering operation range of such devices. Besides, further research could focus on the improvement of reaction kinetics on the anode side, guiding, for instance, the uniform deposition of  $\text{Zn}^{2+}$  on the anode surface. This problem is general for all metal anodes in batteries.

For further study, some additional strategies to improve the overall performance of Zn- $\text{CO}_2$  batteries are proposed: (1) developing high-performance catalytic cathodes with low overpotentials for both  $\text{CO}_2$ -RR and OER; (2) improving the stability of catalytic cathodes, which are capable of standing the repeated reduction and oxidation processes as the bifunctional catalysts; (3) improving the stability of Zn electrodes, which also plays a key role in enhancing the cycling performance of Zn- $\text{CO}_2$  batteries; (4) replacing the BPM with other ion exchange membranes using electrolytes with close pH values on both sides, since the BPM requires an additional voltage of  $\sim 0.83$  V for water dissociation.

In summary, the aqueous Zn- $\text{CO}_2$  battery shows great potential in energy storage and  $\text{CO}_2$  utilization, but current systems are still far from true application, and in-depth research efforts beyond “only” cathodic electrocatalysis are still limited. We however strongly believe that these issues can be successfully addressed in a more holistic fashion, and that Zn- $\text{CO}_2$  batteries have a serious potential as a disruptive device technology on a large scale to switch on demand between  $\text{CO}_2$  utilization and sustainable energy storage.

## Conflicts of interest

The authors declare no conflict of interest.

## Acknowledgements

This work was supported by the National Natural Science Foundation of China (No. 22109044, 52373205, 52003251, 52102166), Natural Science Foundation of Shanghai, China (No. 22ZR1418500), start-up funds from the East China University of Science and Technology, and Henan Center for Outstanding Overseas Scientists (GZS2022014). The computing work in this paper is supported by the Public Service Platform of High Performance Computing by the Network and Computing Center of HUST.

## References

1. D. Schimel, B. B. Stephens and J. B. Fisher, Effect of increasing  $\text{CO}_2$  on the terrestrial carbon cycle, *Proc. Natl. Acad. Sci. U. S. A.*, 2015, **112**, 436–441.
2. S. C. Doney, V. J. Fabry, R. A. Feely and J. A. Kleypas, Ocean acidification: the other  $\text{CO}_2$  problem, *Annu. Rev. Mar. Sci.*, 2009, **1**, 169–192.
3. S. L. Wells and J. DeSimone,  $\text{CO}_2$  technology platform: an important tool for environmental problem solving, *Angew. Chem., Int. Ed.*, 2001, **40**, 518–527.
4. M. Liu, Y. Pang, B. Zhang, P. D. Luna, O. Voznyy, J. Xu, X. Zheng, C. T. Dinh, F. Fan, C. Cao, F. P. G. de Arquer, T. S. Safaei, A. Mepham, A. Klinkova, E. Kumacheva, T. Filleter,



D. Sinton, S. O. Kelley and E. H. Sargent, Enhanced electrocatalytic  $\text{CO}_2$  reduction via field-induced reagent concentration, *Nature*, 2016, **537**, 382–386.

5 Z. Lyu, S. Zhu, M. Xie, Y. Zhang, Z. Chen, R. Chen, M. Tian, M. Chi, M. Shao and Y. Xia, Controlling the surface oxidation of Cu nanowires improves their catalytic selectivity and stability toward  $\text{C}_{2+}$  products in  $\text{CO}_2$  reduction, *Angew. Chem., Int. Ed.*, 2021, **60**, 1909–1915.

6 S. Yang, H. An, S. Arnouts, H. Wang, X. Yu, J. de Ruiter, S. Bals, T. Altantzis, B. M. Weckhuysen and W. van der Stam, Halide-guided active site exposure in bismuth electrocatalysts for selective  $\text{CO}_2$  conversion into formic acid, *Nat. Catal.*, 2023, **6**, 796–806.

7 Y. Li, E. P. Delmo, G. Hou, X. Cui, M. Zhao, Z. Tian, Y. Zhang and M. Shao, Enhancing local  $\text{CO}_2$  adsorption by L-histidine incorporation for selective formate production over the wide potential window, *Angew. Chem., Int. Ed.*, 2023, **62**, e202313522.

8 Z. Wang, Y. Li, X. Zhao, S. Chen, Q. Nian, X. Luo, J. Fan, D. Ruan, B.-Q. Xiong and X. Ren, Localized alkaline environment via in situ electrostatic confinement for enhanced  $\text{CO}_2$ -to-ethylene conversion in neutral medium, *J. Am. Chem. Soc.*, 2023, **145**, 6339–6348.

9 J. Mao, Y. Wang, B. Zhang, Y. Lou, C. Pan, Y. Zhu and Y. Zhang, Advances in electrocarboxylation reactions with  $\text{CO}_2$ , *Green Carbon*, 2024, DOI: [10.1016/j.greanca.2024.02.001](https://doi.org/10.1016/j.greanca.2024.02.001).

10 C. Deng, C. Qi, X. Wu, G. Jing and H. Zhao, Unveiling the relationship between structural evaluation and catalytic performance of InOOH during electroreduction of  $\text{CO}_2$  to formate, *Green Carbon*, 2024, DOI: [10.1016/j.greanca.2024.02.003](https://doi.org/10.1016/j.greanca.2024.02.003).

11 H. Ang, W. Zhang, H. T. Tan, H. Chen and Q. Yan, Copper oxide supported on platinum nanosheets array: high performance carbon-free cathode for lithium-oxygen cells, *J. Power Sources*, 2015, **294**, 377–385.

12 W. Zhang, J. Zhu, H. Ang, H. Wang, H. T. Tan, D. Yang, C. Xu, N. Xiao, B. Li, W. Liu, X. Wang, H. H. Hng and Q. Yan, Fe-based metallopolymer nanowall-based composites for  $\text{Li}-\text{O}_2$  battery cathode, *ACS Appl. Mater. Interfaces*, 2014, **6**, 7164–7170.

13 C. C. Li, W. Zhang, H. Ang, H. Yu, B. Y. Xia, X. Wang, Y. H. Yang, Y. Zhao, H. H. Hng and Q. Yan, Compressed hydrogen gas-induced synthesis of Au-Pt core-shell nanoparticle chains towards high-performance catalysts for  $\text{Li}-\text{O}_2$  batteries, *J. Mater. Chem. A*, 2014, **2**, 10676–10681.

14 W. Zhang, Y. Huang, Y. Liu, L. Wang, S. Chou and H. Liu, Strategies toward stable nonaqueous alkali metal- $\text{O}_2$  batteries, *Adv. Energy Mater.*, 2019, **9**, 1900464.

15 J. Li, Z. Liu, S. Han, P. Zhou, B. Lu, J. Zhou, Z. Zeng, Z. Chen and J. Zhou, Hetero nucleus growth stabilizing zinc anode for high-biosecurity zinc-ion batteries, *Nano-Micro Lett.*, 2023, **15**, 237.

16 X. Xie, J. Li, Z. Xing, B. Lu, S. Liang and J. Zhou, Biocompatible zinc battery with programmable electro-cross-linked electrolyte, *Natl. Sci. Rev.*, 2023, **10**, nwac281.

17 S. Xu, S. K. Das and L. A. Archer, The  $\text{Li}-\text{CO}_2$  battery: a novel method for  $\text{CO}_2$  capture and utilization, *RSC Adv.*, 2013, **3**, 6656–6660.

18 W. I. Al Sadat and L. A. Archer, The  $\text{O}_2$ -assisted  $\text{Al}/\text{CO}_2$  electrochemical cell: a system for  $\text{CO}_2$  capture/conversion and electric power generation, *Sci. Adv.*, 2016, **2**, e1600968.

19 Z. Xie, X. Zhang, Z. Zhang and Z. Zhou, Metal- $\text{CO}_2$  batteries on the road:  $\text{CO}_2$  from contamination gas to energy source, *Adv. Mater.*, 2017, **29**, 1605891.

20 C. J. Fetrow, C. Carugati, X.-D. Zhou and S. Wei, Electrochemistry of metal- $\text{CO}_2$  batteries: opportunities and challenges, *Energy Storage Mater.*, 2022, **45**, 911–933.

21 K. Takechi, T. Shiga and T. Asaoka, A  $\text{Li}-\text{O}_2/\text{CO}_2$  battery, *Chem. Commun.*, 2011, **47**, 3463–3465.

22 S. K. Das, S. Xu and L. A. Archer, Carbon dioxide assist for non-aqueous sodium-oxygen batteries, *Electrochem. Commun.*, 2013, **27**, 59–62.

23 Y. Liu, R. Wang, Y. Lyu, H. Li and L. Chen, Rechargeable  $\text{Li}/\text{CO}_2-\text{O}_2$  (2: 1) battery and  $\text{Li}/\text{CO}_2$  battery, *Energy Environ. Sci.*, 2014, **7**, 677–681.

24 Z. Zhang, X.-G. Wang, X. Zhang, Z. Xie, Y.-N. Chen, L. Ma, Z. Peng and Z. Zhou, Verifying the rechargeability of  $\text{Li}-\text{CO}_2$  batteries on working cathodes of Ni nanoparticles highly dispersed on N-doped graphene, *Adv. Sci.*, 2018, **5**, 1700567.

25 J. Xie, Q. Liu, Y. Huang, M. Wu and Y. Wang, A porous Zn cathode for  $\text{Li}-\text{CO}_2$  batteries generating fuel-gas  $\text{CO}$ , *J. Mater. Chem. A*, 2018, **6**, 13952–13958.

26 Y. Xing, Y. Yang, D. Li, M. Luo, N. Chen, Y. Ye, J. Qian, L. Li, D. Yang, F. Wu, R. Chen and S. Guo, Crumpled Ir nanosheets fully covered on porous carbon nanofibers for long-life rechargeable Lithium- $\text{CO}_2$  batteries, *Adv. Mater.*, 2018, **30**, 1803124.

27 Y. Jiao, J. Qin, H. M. K. Sari, D. Li, X. Li and X. Sun, Recent progress and prospects of  $\text{Li}-\text{CO}_2$  batteries: mechanisms, catalysts and electrolytes, *Energy Storage Mater.*, 2021, **34**, 148–170.

28 C. Xu, Y. Dong, Y. Shen, H. Zhao, L. Li, G. Shao and Y. Lei, Fundamental understanding of nonaqueous and hybrid  $\text{Na}-\text{CO}_2$  batteries: challenges and perspectives, *Small*, 2023, **19**, 2206445.

29 X. Wang, J. Xie, M. A. Ghausi, J. Lv, Y. Huang, M. Wu, Y. Wang and J. Yao, Rechargeable  $\text{Zn}-\text{CO}_2$  electrochemical cells mimicking two-step photosynthesis, *Adv. Mater.*, 2019, **31**, 1807807.

30 R. Yang, J. Xie, Q. Liu, Y. Huang, J. Lv, M. A. Ghausi, X. Wang, Z. Peng, M. Wu and Y. Wang, A trifunctional  $\text{Ni}-\text{N}/\text{P}-\text{O}$ -codoped graphene electrocatalyst enables dual-model rechargeable  $\text{Zn}-\text{CO}_2/\text{Zn}-\text{O}_2$  batteries, *J. Mater. Chem. A*, 2019, **7**, 2575–2580.

31 N. Sreekanth, M. A. Nazrulla, T. V. Vineesh, K. Sailaja and K. L. Phani, Metal-free boron-doped graphene for selective electroreduction of carbon dioxide to formic acid/formate, *Chem. Commun.*, 2015, **51**, 16061–16064.

32 Y. Jia, L. Zhang, A. Du, G. Gao, J. Chen, X. Yan, C. L. Brown and X. Yao, Defect graphene as a trifunctional catalyst for electrochemical reactions, *Adv. Mater.*, 2016, **28**, 9532–9538.



33 J. Xie, X. Wang, J. Lv, Y. Huang, M. Wu, Y. Wang and J. Yao, Reversible aqueous Zinc–CO<sub>2</sub> batteries based on CO<sub>2</sub>–HCOOH interconversion, *Angew. Chem., Int. Ed.*, 2018, **57**, 16996–17001.

34 X. Hao, X. An, A. M. Patil, P. Wang, X. Ma, X. Du, X. Hao, A. Abudula and G. Guan, Biomass-derived N-doped carbon for efficient electrocatalytic CO<sub>2</sub> reduction to CO and Zn–CO<sub>2</sub> batteries, *ACS Appl. Mater. Interfaces*, 2021, **13**, 3738–3747.

35 S. Kaur, M. Kumar, D. Gupta, P. P. Mohanty, T. Das, S. Chakraborty, R. Ahuja and T. C. Nagaiah, Efficient CO<sub>2</sub> utilization and sustainable energy conversion via aqueous Zn–CO<sub>2</sub> batteries, *Nano Energy*, 2023, **109**, 108242.

36 W. Zheng, D. Wang, Y. Zhang, S. Zheng, B. Yang, Z. Li, R. D. Rodriguez, T. Zhang, L. Lei, S. Yao and Y. Hou, Promoting industrial-level CO<sub>2</sub> electroreduction kinetics via accelerating proton feeding on a metal-free aerogel electrocatalyst, *Nano Energy*, 2023, **105**, 107980.

37 W. Yang, Z. Xue, J. Yang, J. Xian, Q. Liu, Y. Fan, K. Zheng, P. Liao, H. Su, Q. Liu, G. Li and C.-Y. Su, Fe nanoparticles embedded in N-doped porous carbon for enhanced electrocatalytic CO<sub>2</sub> reduction and Zn–CO<sub>2</sub> battery, *Chin. J. Catal.*, 2023, **48**, 185–194.

38 X. Teng, J. Lu, Y. Niu, S. Gong, M. Xu, T. J. Meyer and Z. Chen, Selective CO<sub>2</sub> reduction to formate on a Zn-based electrocatalyst promoted by tellurium, *Chem. Mater.*, 2022, **34**, 6036–6047.

39 J. Wang, Z. Li, Z. Zhu, J. Jiang, Y. Li, J. Chen, X. Niu, J. S. Chen and R. Wu, Tailoring the interactions of heterostructured Ni<sub>4</sub>N/Ni<sub>3</sub>ZnC<sub>0.7</sub> for efficient CO<sub>2</sub> electroreduction, *J. Energy Chem.*, 2022, **75**, 1–7.

40 D. Xiang, K. Li, K. Miao, R. Long, Y. Xiong and X. Kang, Amine-functionalized Copper catalysts: hydrogen bonding mediated electrochemical CO<sub>2</sub> reduction to C<sub>2</sub> products and superior rechargeable Zn–CO<sub>2</sub> battery performance, *Acta Phys.-Chim. Sin.*, 2024, **40**(8), 2308027.

41 H. Liao, H. Xie, S. Zhai, L. Fu, Y. Zhang, S. Hao, B. Chen, C. He and Z. Shao, A partially Fe-substituted perovskite electrode for enhancing Zn–CO<sub>2</sub> batteries, *Chem. Eng. J.*, 2023, **474**, 145594.

42 L. Han, X. Peng, H.-T. Wang, P. Ou, Y. Mi, C.-W. Pao, J. Zhou, J. Wang, X. Liu, W.-F. Pong, J. Song, Z. Lin, J. Luo and H. L. Xin, Chemically coupling SnO<sub>2</sub> quantum dots and MXene for efficient CO<sub>2</sub> electroreduction to formate and Zn–CO<sub>2</sub> battery, *Proc. Natl. Acad. Sci. U. S. A.*, 2022, **119**, e2207326119.

43 M. Yang, S. Liu, J. Sun, M. Jin, R. Fu, S. Zhang, H. Li, Z. Sun, J. Luo and X. Liu, Highly dispersed Bi clusters for efficient rechargeable Zn–CO<sub>2</sub> batteries, *Appl. Catal., B*, 2022, **307**, 121145.

44 Y. Wang, L. Xu, L. Zhan, P. Yang, S. Tang, M. Liu, X. Zhao, Y. Xiong, Z. Chen and Y. Lei, Electron accumulation enables Bi efficient CO<sub>2</sub> reduction for formate production to boost clean Zn–CO<sub>2</sub> batteries, *Nano Energy*, 2022, **92**, 106780.

45 X. Hu, Y. Liu, W. Cui, X. Yang, J. Li, S. Zheng, B. Yang, Z. Li, X. Sang, Y. Li, L. Lei and Y. Hou, Boosting industrial-level CO<sub>2</sub> electroreduction of N-doped carbon nanofibers with confined Tin-Nitrogen active sites via accelerating proton transport kinetics, *Adv. Funct. Mater.*, 2023, **33**, 2208781.

46 W. Wang, S. Gong, R. Lu, H. Wang, J. Liu, X. Zhu, B. Liu and X. Lv, In situ growth of Ag aerogels mediating effective electrocatalytic CO<sub>2</sub> reduction and Zn–CO<sub>2</sub> batteries, *Chem. Eng. Sci.*, 2023, **280**, 119042.

47 S. S. Gao, M. M. Jin, J. Q. Sun, X. J. Liu, S. S. Zhang, H. Y. Li, J. Luo and X. P. Sun, Coralloid Au enables high-performance Zn–CO<sub>2</sub> battery and self-driven CO production, *J. Mater. Chem. A*, 2021, **9**, 21024–21031.

48 S. Gao, S. Chen, Q. Liu, S. Zhang, G. Qi, J. Luo and X. Liu, Bifunctional BiPd alloy particles anchored on carbon matrix for reversible Zn–CO<sub>2</sub> battery, *ACS Appl. Nano Mater.*, 2022, **5**, 12387–12394.

49 S. Liu, M. Jin, J. Sun, Y. Qin, S. Gao, Y. Chen, S. Zhang, J. Luo and X. Liu, Coordination environment engineering to boost electrocatalytic CO<sub>2</sub> reduction performance by introducing boron into single-Fe-atomic catalyst, *Chem. Eng. J.*, 2022, **437**, 135294.

50 S. Chen, J. Chen, Y. Li, S. Tan, X. Liao, T. Zhao, K. Zhang, E. Hu, F. Cheng and H. Wang, Fe–N<sub>4</sub>O–C nanoplates covalently bonding on graphene for efficient CO<sub>2</sub> electroreduction and Zn–CO<sub>2</sub> batteries, *Adv. Funct. Mater.*, 2023, **33**, 2300801.

51 S. Gong, W. Wang, C. Zhang, M. Zhu, R. Lu, J. Ye, H. Yang, C. Wu, J. Liu, D. Rao, S. Shao and X. Lv, Tuning the metal electronic structure of anchored cobalt phthalocyanine via dual-regulator for efficient CO<sub>2</sub> electroreduction and Zn–CO<sub>2</sub> batteries, *Adv. Funct. Mater.*, 2022, **32**, 2110649.

52 J. Li, L.-W. Chen, Y.-C. Hao, M. Yuan, J. Lv, A. Dong, S. Li, H. Gu, A.-X. Yin, W. Chen, P. Li and B. Wang, Asymmetric coordinated single-atom Pd sites for high performance CO<sub>2</sub> electroreduction and Zn–CO<sub>2</sub> battery, *Chem. Eng. J.*, 2023, **461**, 141865.

53 D. Lin, T. Wang, Z. Zhao, Y. Liu, H. Song, X. Yang, Z. Li, S. Yao, X. Hu, L. Lei, B. Yang and Y. Hou, Molten-salt-assisted synthesis of single-atom iron confined N-doped carbon nanosheets for highly efficient industrial-level CO<sub>2</sub> electroreduction and Zn–CO<sub>2</sub> batteries, *Nano Energy*, 2023, **113**, 108568.

54 M. K. Aslam, H. Wang, S. Chen, Q. Li and J. Duang, Progress and perspectives of metal (Li, Na, Al, Zn and K)–CO<sub>2</sub> batteries, *Mater. Today Energy*, 2023, **31**, 101196.

55 J. Xie, Z. Zhou and Y. Wang, Metal–CO<sub>2</sub> batteries at the crossroad to practical energy storage and CO<sub>2</sub> recycle, *Adv. Funct. Mater.*, 2020, **30**, 1908285.

56 S. Ibraheem, S. Chen, J. Li, W. Li, X. Gao, Q. Wang and Z. Wei, Three-dimensional Fe,N-decorated carbon-supported NiFeP nanoparticles as an efficient bifunctional catalyst for rechargeable Zinc–O<sub>2</sub> batteries, *ACS Appl. Mater. Interfaces*, 2019, **11**, 699–705.

57 Y. Liu, Y. An, J. Zhu, L. Zhu, X. Li, P. Gao, G. He and Q. Pang, Integrated energy storage and CO<sub>2</sub> conversion using



an aqueous battery with tamed asymmetric reactions, *Nat. Commun.*, 2024, **15**, 977.

58 S. Liang, N. Altaf, L. Huang, Y. Gao and Q. Wang, Electrolytic cell design for electrochemical  $\text{CO}_2$  reduction, *J. CO<sub>2</sub> Util.*, 2020, **35**, 90–105.

59 Y. Xie, P. Ou, X. Wang, Z. Xu, Y. Li, Z. Wang, J. Huang, J. Wicks, C. McCallum, N. Wang, Y. Wang, T. Chen, B. Lo, D. Sinton, J. Yu, Y. Wang and E. Sargent, High carbon utilization in  $\text{CO}_2$  reduction to multi-carbon products in acidic media, *Nat. Catal.*, 2022, **5**, 564–570.

60 X. Zou and J. Gu, Strategies for efficient  $\text{CO}_2$  electroreduction in acidic conditions, *Chin. J. Catal.*, 2023, **52**, 14–31.

61 K. Wang, Y. Wu, X. Cao, L. Gu and J. Hu, A Zn– $\text{CO}_2$  flow battery generating electricity and methane, *Adv. Funct. Mater.*, 2020, **30**, 1908965.

62 D. S. Su, J. Zhang, B. Frank, A. Thomas, X. Wang, J. Paraknowitsch and R. Schlögl, Metal-free heterogeneous catalysis for sustainable chemistry, *ChemSusChem*, 2010, **3**, 169–180.

63 J. Wu, W. Pisula and K. Müllen, Graphenes as potential material for electronics, *Chem. Rev.*, 2007, **107**, 718–747.

64 X.-K. Kong, Z.-Y. Sun, M. Chen, C.-L. Chen and Q.-W. Chen, Metal-free catalytic reduction of 4-nitrophenol to 4-aminophenol by N-doped graphene, *Energy Environ. Sci.*, 2013, **6**, 3260–3266.

65 K. Gong, F. Du, Z. Xia, M. Durstock and L. Dai, Nitrogen-doped carbon nanotube arrays with high electrocatalytic activity for oxygen reduction, *Science*, 2009, **323**, 760–764.

66 E. Gottlieb, K. Matyjaszewski and T. Kowalewski, Polymer-based synthetic routes to carbon-based metal-free catalysts, *Adv. Mater.*, 2019, **31**, 1804626.

67 H. Wang, Y. Chen, X. Hou, C. Ma and T. Tan, Nitrogen-doped graphenes as efficient electrocatalysts for the selective reduction of carbon dioxide to formate in aqueous solution, *Green Chem.*, 2016, **18**, 3250–3256.

68 X. Duan, J. Xu, Z. Wei, J. Ma, S. Guo, S. Wang, H. Liu and S. Dou, Metal-free carbon materials for  $\text{CO}_2$  electrochemical reduction, *Adv. Mater.*, 2017, **29**, 1701784.

69 S. Gao, Y. Liu, Z. Xie, Y. Qiu, L. Zhuo, Y. Qin, J. Ren, S. Zhang, G. Hu, J. Luo and X. Liu, Metal-free bifunctional ordered mesoporous carbon for reversible Zn– $\text{CO}_2$  batteries, *Small Methods*, 2021, **5**, 2001039.

70 C. Chen, X. Sun, X. Yan, Y. Wu, H. Liu, Q. Zhu, B. B. A. Bediako and B. Han, Boosting  $\text{CO}_2$  electroreduction on N, P-Co-doped carbon aerogels, *Angew. Chem.*, 2020, **132**, 11216–11222.

71 H. Yang, Y. Wu, Q. Lin, L. Fan, X. Chai, Q. Zhang, J. Liu, C. He and Z. Lin, Composition tailoring via N and S Co-doping and structure tuning by constructing hierarchical pores: metal-free catalysts for high-performance electrochemical reduction of  $\text{CO}_2$ , *Angew. Chem.*, 2018, **130**, 15702.

72 Y. Zhang, X. Wang, S. Zheng, B. Yang, Z. Li, J. Lu, Q. Zhang, N. M. Adli, L. Lei, G. Wu and Y. Hou, Hierarchical cross-linked carbon aerogels with transition metal-nitrogen sites for highly efficient industrial-level  $\text{CO}_2$  electroreduction, *Adv. Funct. Mater.*, 2021, **31**, 2104377.

73 D. R. Chen, M. Chitranshi, V. Shanov and M. Schulz, Electrochemically activated CNT sheet as a cathode for Zn– $\text{CO}_2$  batteries, *Int. J. Mol. Sci.*, 2022, **23**, 12602.

74 F. Pan, W. Deng, C. Justiniano and Y. Li, Identification of champion transition metals centers in metal and nitrogen-codoped carbon catalysts for  $\text{CO}_2$  reduction, *Appl. Catal., B*, 2018, **226**, 463–472.

75 T. N. Huan, N. Ranjbar, G. Rousse, M. Sougrati, A. Zitolo, V. Mougel, F. Jaouen and M. Fontecave, Electrochemical reduction of  $\text{CO}_2$  catalyzed by Fe-N-C materials: a structure-selectivity study, *ACS Catal.*, 2017, **7**, 1520–1525.

76 Y. Qu, Z. Li, W. Chen, Y. Lin, T. Yuan, Z. Yang, C. Zhao, J. Wang, C. Zhao, X. Wang, F. Zhou, Z. Zhuang, Y. Wu and Y. Li, Direct transformation of bulk copper into copper single sites via emitting and trapping of atoms, *Nat. Catal.*, 2018, **1**, 781–786.

77 Y. Mun, K. Kim, S. Kim, S. Lee, S. Lee, W. Choi, S. Kim, J. Han and J. Lee, A novel strategy to develop non-noble metal catalyst for  $\text{CO}_2$  electroreduction: hybridization of metal-organic polymer, *Appl. Catal., B*, 2018, **236**, 154–161.

78 S. Liang, L. Huang, Y. Gao, Q. Wang and B. Liu, Electrochemical reduction of  $\text{CO}_2$  to CO over transition metal/N-doped carbon catalysts: the active sites and reaction mechanism, *Adv. Sci.*, 2021, **8**, 2102886.

79 H.-J. Zhu, M. Lu, Y.-R. Wang, S.-J. Yao, M. Zhang, Y.-H. Kan, J. Liu, Y. Chen, S.-L. Li and Y.-Q. Lan, Efficient electron transmission in covalent organic framework nanosheets for highly active electrocatalytic carbon dioxide reduction, *Nat. Commun.*, 2020, **11**, 497.

80 A. E. Baumann, D. A. Burns, B. Liu and V. S. Thoi, Metal-organic framework functionalization and design strategies for advanced electrochemical energy storage devices, *Commun. Chem.*, 2019, **2**, 86.

81 Q. Ren, H. Wang, X.-F. Lu, Y.-X. Tong and G.-R. Li, Recent progress on MOF-derived heteroatom-doped carbon-based electrocatalysts for oxygen reduction reaction, *Adv. Sci.*, 2018, **5**, 1700515.

82 Y. V. Kaneti, J. Tang, R. R. Salunkhe, X. Jiang, A. Yu, K. C. W. Wu and Y. Yamauchi, Nanoarchitected design of porous materials and nanocomposites from metal-organic frameworks, *Adv. Mater.*, 2017, **29**, 1604898.

83 M. Liu, X. Lu, C. Guo, Z. Wang, Y. Li, Y. Lin, Y. Zhou, S. Wang and J. Zhang, Architecting a mesoporous N-doped graphitic carbon framework encapsulating  $\text{CoTe}_2$  as an efficient oxygen evolution electrocatalyst, *ACS Appl. Mater. Interfaces*, 2017, **9**, 36146–36153.

84 F. Wang, G. Wang, P. Deng, Y. Chen, J. Li, D. Wu, Z. Wang, C. Wang, Y. Hua and X. Tian, Ultrathin nitrogen-doped carbon encapsulated Ni nanoparticles for highly efficient electrochemical  $\text{CO}_2$  reduction and aqueous Zn– $\text{CO}_2$  batteries, *Small*, 2023, **19**, 2301128.

85 M. Sun, H. Liu, J. Qu and J. Li, Earth-rich transition metal phosphide for energy conversion and storage, *Adv. Energy Mater.*, 2016, **6**, 1600087.



86 M. Peng, S. Ci, P. Shao, P. Cai and Z. Wen, Cu<sub>3</sub>P/C nanocomposites for efficient electrocatalytic CO<sub>2</sub> reduction and Zn-CO<sub>2</sub> battery, *J. Nanosci. Nanotechnol.*, 2019, **19**, 3232–3236.

87 K. P. Singh, E. J. Bae and J.-S. Yu, Fe-P: a new class of electroactive catalyst for oxygen reduction reaction, *J. Am. Chem. Soc.*, 2015, **137**, 3165–3168.

88 S. Liu, L. Wang, H. Yang, S. Gao, Y. Liu, S. Zhang, Y. Chen, X. Liu and J. Luo, Nitrogen-doped carbon polyhedrons confined Fe-P nanocrystals as high-efficiency bifunctional catalysts for aqueous Zn-CO<sub>2</sub> batteries, *Small*, 2022, **18**, 2104965.

89 D.-H. Guan, X.-X. Wang, M.-L. Li, F. Li, L.-J. Zheng, X.-L. Huang and J.-J. Xu, Light/electricity energy conversion and storage for a hierarchical porous In<sub>2</sub>S<sub>3</sub>@CNT/SS cathode towards a flexible Li-CO<sub>2</sub> battery, *Angew. Chem., Int. Ed.*, 2020, **59**, 19518–19524.

90 Z. Li, M.-L. Li, X.-X. Wang, D.-H. Guan, W.-Q. Liu and J.-J. Xu, In situ fabricated photo-electro-catalytic hybrid cathode for light-assisted lithium-CO<sub>2</sub> batteries, *J. Mater. Chem. A*, 2020, **8**, 14799–14806.

91 Z. Zhu, X. Shi, G. Fan, F. Li and J. Chen, Photo-energy conversion and storage in an aprotic Li-O<sub>2</sub> battery, *Angew. Chem.*, 2019, **131**, 19197–19202.

92 K. Wang, Z. Mo, S. Tang, M. Li, H. Yang, B. Long, Y. Wang, S. Song and Y. Tong, Photo-enhanced Zn-air batteries with simultaneous highly efficient in situ H<sub>2</sub>O<sub>2</sub> generation for wastewater treatment, *J. Mater. Chem. A*, 2019, **7**, 14129–14135.

93 X. Liu, S. Tao, J. Zhang, Y. Zhu, R. Ma and J. Lu, Ultrathin p-n type Cu<sub>2</sub>O/CuCoCr-layered double hydroxide heterojunction nanosheets for photo-assisted aqueous Zn-CO<sub>2</sub> batteries, *J. Mater. Chem. A*, 2021, **9**, 26061–26068.

94 J. Fan, X. Zhao, X. Mao, J. Xu, N. Han, H. Yang, B. Pan, Y. Li, L. Wang and Y. Li, Large-area vertically aligned bismuthene nanosheet arrays from galvanic replacement reaction for efficient electrochemical CO<sub>2</sub> conversion, *Adv. Mater.*, 2021, **33**, 2100910.

95 Y. Wang, Z. Huang, Y. Lei, J. Wu, Y. Bai, X. Zhao, M. Liu, L. Zhan, S. Tang, X. Zhang, F. Luo and X. Xiong, Bismuth with abundant defects for electrocatalytic CO<sub>2</sub> reduction and Zn-CO<sub>2</sub> batteries, *Chem. Commun.*, 2022, **58**, 3621–3624.

96 H. Wang, M. K. Aslam, Z. Nie, K. Yang, X. Li, S. Chen, Q. Li, D. Chao and J. Duan, Dual-anion regulation for reversible and energetic aqueous Zn-CO<sub>2</sub> batteries, *Small Methods*, 2023, 2300867.

97 W. Wu, J. Zhu, Y. Tong, S. Xiang and P. Chen, Electronic structural engineering of bimetallic Bi-Cu alloying nanosheet for highly-efficient CO<sub>2</sub> electroreduction and Zn-CO<sub>2</sub> batteries, *Nano Res.*, 2024, **17**, 3684–3692.

98 A. Xu, X. Chen, D. Wei, B. Chu, M. Yu, X. Yin and J. Xu, Regulating the electronic structure of bismuth nanosheets by titanium doping to boost CO<sub>2</sub> electroreduction and Zn-CO<sub>2</sub> batteries, *Small*, 2023, **19**, 2302253.

99 Q. Wang, X. Yang, H. Zang, C. Liu, J. Wang, N. Yu, L. Kuai, Q. Qin and B. Geng, InBi bimetallic sites for efficient electrochemical reduction of CO<sub>2</sub> to HCOOH, *Small*, 2023, **19**, 2303172.

100 Y. Huang, X. Mao, G. Yuan, D. Zhang, B. Pan, J. Deng, Y. Shi, N. Han, C. Li, L. Zhang, L. Wang, L. He, Y. Li and Y. Li, Size-dependent selectivity of electrochemical CO<sub>2</sub> reduction on converted In<sub>2</sub>O<sub>3</sub> nanocrystals, *Angew. Chem.*, 2021, **133**, 15978–15982.

101 X. Zheng, P. De Luna, F. P. García de Arquer, B. Zhang, N. Becknell, M. B. Ross, Y. Li, M. N. Banis, Y. Li, M. Liu, O. Voznyy, C. T. Dinh, T. Zhuang, P. Stadler, Y. Cui, X. Du, P. Yang and E. H. Sargent, Sulfur-modulated tin sites enable highly selective electrochemical reduction of CO<sub>2</sub> to formate, *Joule*, 2017, **1**, 794–805.

102 S. Liu, J. Xiao, X. F. Lu, J. Wang, X. Wang and X. W. Lou, Efficient electrochemical reduction of CO<sub>2</sub> to HCOOH over Sub-2 nm SnO<sub>2</sub> quantum wires with exposed grain boundaries, *Angew. Chem., Int. Ed.*, 2019, **58**, 8499–8503.

103 X. Teng, Y. Niu, S. Gong, M. Xu, X. Liu, L. Ji and Z. Chen, In/ZnO@C hollow nanocubes for efficient electrochemical reduction of CO<sub>2</sub> to formate and rechargeable Zn-CO<sub>2</sub> batteries, *Mater. Chem. Front.*, 2021, **5**, 6618–6627.

104 Z. Li, A. Cao, Q. Zheng, Y. Fu, T. Wang, K. T. Arul, J.-L. Chen, B. Yang, N. M. Adli, L. Lei, C.-L. Dong, J. Xiao, G. Wu and Y. Hou, Elucidation of the synergistic effect of dopants and vacancies on promoted selectivity for CO<sub>2</sub> electroreduction to formate, *Adv. Mater.*, 2021, **33**, 2005113.

105 W. Ni, Y. Gao, Y. Lin, C. Ma, X. Guo, S. Wang and S. Zhang, Nonnitrogen coordination environment steering electrochemical CO<sub>2</sub>-to-CO conversion over single-atom tin catalysts in a wide potential window, *ACS Catal.*, 2021, **11**, 5212–5221.

106 Y. Shi, Z. Lyu, M. Zhao, R. Chen, Q. N. Nguyen and Y. Xia, Noble-metal nanocrystals with controlled shapes for catalytic and electrocatalytic applications, *Chem. Rev.*, 2021, **121**, 649–735.

107 Y. Chen, C. W. Li and M. W. Kanan, Aqueous CO<sub>2</sub> reduction at very low overpotential on oxide-derived Au nanoparticles, *J. Am. Chem. Soc.*, 2012, **134**, 19969–19972.

108 D. Mateo, I. Esteve-Adell, J. Albero, J. F. S. Royo, A. Primo and H. Garcia, 111 oriented gold nanoplatelets on multilayer graphene as visible light photocatalyst for overall water splitting, *Nat. Commun.*, 2016, **7**, 11819.

109 N. Hoshi, T. Mizumura and Y. Hori, Significant difference of the reduction rates of carbon dioxide between Pt(111) and Pt(110) single crystal electrodes, *Electrochim. Acta*, 1995, **40**, 883–887.

110 S. Mezzavilla, S. Horch, I. E. L. Stephens, B. Seger and I. Chorkendorff, Structure sensitivity in the electrocatalytic reduction of CO<sub>2</sub> with gold catalysts, *Angew. Chem.*, 2019, **131**, 3814–3818.

111 S. Dai, T.-H. Huang, W.-I. Liu, C.-W. Hsu, S.-W. Lee, T.-Y. Chen, Y.-C. Wang, J.-H. Wang and K.-W. Wang, Enhanced CO<sub>2</sub> electrochemical reduction performance over Cu@AuCu catalysts at high noble metal utilization efficiency, *Nano Lett.*, 2021, **21**, 9293–9300.



112 A. R. Woldu, From low to high-index facets of noble metal nanocrystals: a way forward to enhance the performance of electrochemical  $\text{CO}_2$  reduction, *Nanoscale*, 2020, **12**, 8626–8635.

113 J. Wang, S. Kattel, C. J. Hawhurst, J. H. Lee, B. M. Tackett, K. Chang, N. Rui, C.-J. Liu and J. G. Chen, Enhancing activity and reducing cost for electrochemical reduction of  $\text{CO}_2$  by supporting palladium on metal carbides, *Angew. Chem., Int. Ed.*, 2019, **58**, 6271–6275.

114 X. Huang, X. Zhou, S. Wu, Y. Wei, X. Qi, J. Zhang, F. Boey and H. Zhang, Reduced graphene oxide-templated photochemical synthesis and in situ assembly of Au nanodots to orderly patterned Au nanodot chains, *Small*, 2010, **6**, 513–516.

115 S. Gao, S. Hao, Z. Huang, Y. Yuan, S. Han, L. Lei, X. Zhang, R. Shahbazian-Yassar and J. Lu, Synthesis of high-entropy alloy nanoparticles on supports by the fast moving bed pyrolysis, *Nat. Commun.*, 2020, **11**, 2016.

116 S. Gao, M. Jin, J. Sun, X. Liu, S. Zhang, H. Li, J. Luo and X. Sun, Coralloid Au enables high-performance  $\text{Zn}-\text{CO}_2$  battery and self-driven CO production, *J. Mater. Chem. A*, 2021, **9**, 21024–21031.

117 V. Celorio, P. M. Quaino, E. Santos, J. Flórez-Montaño, J. J. L. Humphrey, O. Guillén-Villafuerte, D. Plana, M. J. Lázaro, E. Pastor and D. J. Fermín, Strain effects on the oxidation of CO and  $\text{HCOOH}$  on Au-Pd core-shell nanoparticles, *ACS Catal.*, 2017, **7**, 1673–1680.

118 D. Gao, H. Zhou, F. Cai, D. Wang, Y. Hu, B. Jiang, W.-B. Cai, X. Chen, R. Si, F. Yang, S. Miao, J. Wang, G. Wang and X. Bao, Switchable  $\text{CO}_2$  electroreduction via engineering active phases of Pd nanoparticles, *Nano Res.*, 2017, **10**, 2181–2191.

119 S. Yang, J. Kim, Y. J. Tak, A. Soon and H. Lee, Single-atom catalyst of platinum supported on titanium nitride for selective electrochemical reactions, *Angew. Chem., Int. Ed.*, 2016, **55**, 2058–2062.

120 Y. H. Li, S. N. Zhao and S. Q. Zang, Programmable kernel structures of atomically precise metal nanoclusters for tailoring catalytic properties, *Exploration*, 2023, **3**, 20220005.

121 T. Tang, Z. Wang and J. Guan, Achievements and challenges of copper-based single-atom catalysts for the reduction of carbon dioxide to  $\text{C}_{2+}$  products, *Exploration*, 2023, **3**, 20230011.

122 J. Wu, L. Xiong, B. Zhao, M. Liu and L. Huang, Densely populated single atom catalysts, *Small Methods*, 2020, **4**, 1900540.

123 L. Zhao, Y. Zhang, L.-B. Huang, X.-Z. Liu, Q.-H. Zhang, C. He, Z.-Y. Wu, L.-J. Zhang, J. Wu, W. Yang, L. Gu, J.-S. Hu and L.-J. Wan, Cascade anchoring strategy for general mass production of high-loading single-atomic metal-nitrogen catalysts, *Nat. Commun.*, 2019, **10**, 1278.

124 G. Zhang, Y. Jia, C. Zhang, X. Xiong, K. Sun, R. Chen, W. Chen, Y. Kuang, L. Zheng, H. Tang, W. Liu, J. Liu, X. Sun, W.-F. Lin and H. Dai, A general route via formamide condensation to prepare atomically dispersed metal-nitrogen–carbon electrocatalysts for energy technologies, *Energy Environ. Sci.*, 2019, **12**, 1317–1325.

125 J. Jones, H. Xiong, A. T. DeLaRiva, E. J. Peterson, H. Pham, S. R. Challa, G. Qi, S. Oh, M. H. Wiebenga, X. I. Pereira Hernández, Y. Wang and A. K. Datye, Thermally stable single-atom platinum-on-ceria catalysts via atom trapping, *Science*, 2016, **353**, 150–154.

126 Y. Pan, S. Liu, K. Sun, X. Chen, B. Wang, K. Wu, X. Cao, W.-C. Cheong, R. Shen, A. Han, Z. Chen, L. Zheng, J. Luo, Y. Lin, Y. Liu, D. Wang, Q. Peng, Q. Zhang, C. Chen and Y. Li, A bimetallic  $\text{Zn}/\text{Fe}$  polyphthalocyanine-derived single-atom  $\text{Fe}-\text{N}_4$  catalytic site: a superior trifunctional catalyst for overall water splitting and  $\text{Zn}-\text{Air}$  batteries, *Angew. Chem., Int. Ed.*, 2018, **57**, 8614–8618.

127 J. Chen, H. Li, C. Fan, Q. Meng, Y. Tang, X. Qiu, G. Fu and T. Ma, Dual single-atomic  $\text{Ni}-\text{N}_4$  and  $\text{Fe}-\text{N}_4$  sites constructing janus hollow graphene for selective oxygen electrocatalysis, *Adv. Mater.*, 2020, **32**, 2003134.

128 Z. Zeng, A. G. Mohamed, A. X. Zhang and Y. Wang, Wide potential  $\text{CO}_2$ -to-CO electroreduction relies on pyridinic-N/ $\text{Ni}-\text{N}_x$  sites and its  $\text{Zn}-\text{CO}_2$  battery application, *Energy Technol.*, 2021, **9**, 2100205.

129 C. Zhao, X. Dai, T. Yao, W. Chen, X. Wang, J. Wang, J. Yang, S. Wei, Y. Wu and Y. Li, Ionic exchange of metal–organic frameworks to access single nickel sites for efficient electroreduction of  $\text{CO}_2$ , *J. Am. Chem. Soc.*, 2017, **139**, 8078–8081.

130 X. Li, W. Bi, M. Chen, Y. Sun, H. Ju, W. Yan, J. Zhu, X. Wu, W. Chu, C. Wu and Y. Xie, Exclusive  $\text{Ni}-\text{N}_4$  sites realize near-unity CO selectivity for electrochemical  $\text{CO}_2$  reduction, *J. Am. Chem. Soc.*, 2017, **139**, 14889–14892.

131 Y. Pan, R. Lin, Y. Chen, S. Liu, W. Zhu, X. Cao, W. Chen, K. Wu, W.-C. Cheong, Y. Wang, L. Zheng, J. Luo, Y. Lin, Y. Liu, C. Liu, J. Li, Q. Lu, X. Chen, D. Wang, Q. Peng, C. Chen and Y. Li, Design of single-atom  $\text{Co}-\text{N}_5$  catalytic site: a robust electrocatalyst for  $\text{CO}_2$  reduction with nearly 100% CO selectivity and remarkable stability, *J. Am. Chem. Soc.*, 2018, **140**, 4218–4221.

132 Y. Zhang, L. Jiao, W. Yang, C. Xie and H.-L. Jiang, Rational fabrication of low-coordinate single-atom Ni electrocatalysts by MOFs for highly selective  $\text{CO}_2$  reduction, *Angew. Chem., Int. Ed.*, 2021, **60**, 7607–7611.

133 J. Chen, Z. Li, X. Wang, X. Sang, S. Zheng, S. Liu, B. Yang, Q. Zhang, L. Lei, L. Dai and Y. Hou, Promoting  $\text{CO}_2$  electroreduction kinetics on atomically dispersed monovalent  $\text{ZnI}$  sites by rationally engineering proton-feeding centers, *Angew. Chem., Int. Ed.*, 2022, **61**, e202111683.

134 Z. Li, R. Wu, S. Xiao, Y. Yang, L. Lai, J. S. Chen and Y. Chen, Axial chlorine coordinated iron-nitrogen-carbon single-atom catalysts for efficient electrochemical  $\text{CO}_2$  reduction, *Chem. Eng. J.*, 2022, **430**, 132882.

135 Y. Zhao, Z. Pei, X. F. Lu, D. Luan, X. Wang and X. W. Lou, Rationally designed nitrogen-doped carbon macroporous



fibers with loading of single cobalt sites for efficient aqueous Zn-CO<sub>2</sub> batteries, *Chem Catal.*, 2022, **2**, 1480–1493.

136 J. Gu, C.-S. Hsu, L. Bai, H. M. Chen and X. Hu, Atomically dispersed Fe<sup>3+</sup> sites catalyze efficient CO<sub>2</sub> electroreduction to CO, *Science*, 2019, **364**, 1091–1094.

137 C. Zhang, S. Yang, J. Wu, M. Liu, S. Yazdi, M. Ren, J. Sha, J. Zhong, K. Nie, A. S. Jalilov, Z. Li, H. Li, B. I. Yakobson, Q. Wu, E. Ringe, H. Xu, P. M. Ajayan and J. M. Tour, Electrochemical CO<sub>2</sub> reduction with atomic Iron-dispersed on nitrogen-doped graphene, *Adv. Energy Mater.*, 2018, **8**, 1703487.

138 W. Ni, Z. Liu, Y. Zhang, C. Ma, H. Deng, S. Zhang and S. Wang, Electroreduction of carbon dioxide driven by the intrinsic defects in the carbon plane of a single Fe-N<sub>4</sub> site, *Adv. Mater.*, 2021, **33**, 2003238.

139 C. Guo, T. Zhang, X. Liang, X. Deng, W. Guo, Z. Wang, X. Lu and C.-M. L. Wu, Single transition metal atoms on nitrogen-doped carbon for CO<sub>2</sub> electrocatalytic reduction: CO production or further CO reduction?, *Appl. Surf. Sci.*, 2020, **533**, 147466.

140 W. Ju, A. Bagger, X. Wang, Y. Tsai, F. Luo, T. Möller, H. Wang, J. Rossmeisl, A. S. Varela and P. Strasser, Unraveling mechanistic reaction pathways of the electrochemical CO<sub>2</sub> reduction on Fe-N-C single-site catalysts, *ACS Energy Lett.*, 2019, **4**, 1663–1671.

